JOURNAL OF GEOPHYSICAL RESEARCH: OCEANS, VOL. 118, 4822–4838, doi:10.1002/jgrc.20362, 2013

Nutrient distributions, transports, and budgets on the inner margin of a river-dominated continental shelf

John C. Lehrter,[1] Dong S. Ko,[2] Michael C. Murrell,[1] James D. Hagy,[1] Blake A. Schaeffer,[1] Richard M. Greene,[1] Richard W. Gould,[2] and Bradley Penta[2]

Received 18 March 2013; revised 23 July 2013; accepted 16 August 2013; published 2 October 2013.

[1] Physical and biogeochemical processes determining the distribution, transport, and fate of nutrients delivered by the Mississippi and Atchafalaya river basin (MARB) to the inner Louisiana continental shelf (LCS) were examined using a three-dimensional hydrodynamic model and observations of hydrography, nutrients, and organic carbon collected during 12 cruises. Two aspects of nutrient transport and fate on the inner LCS (<50 m depth) were evaluated: (1) along-shelf and cross-shelf transports were calculated and (2) nutrient sinks and sources were inferred. On average, 47% of the lower Mississippi River freshwater traveled westward on the LCS, but this percentage was reduced during summer when currents reversed to a predominately upcoast direction. Changes from mainly inorganic to organic nutrients were observed at salinity between 20 and 30, and above 30, organic nutrients were the dominant forms. Westward transport of dissolved inorganic nitrogen (DIN) was about 25% of the combined DIN load from the MARB, whereas westward transport of dissolved organic nitrogen (DON) was 2.8-fold larger than the MARB DON load. Different from dissolved inorganic nutrients, for which the rivers were the primary source, the dominant source of organic nutrients was advection from offshore. Overall, the inner LCS was estimated to be a net sink for total nitrogen in the amount of −3.14 mmol N m^{-2} d^{-1} and a net sink for total phosphorus in the amount of −0.28 mmol P m^{-2} d^{-1}. These sinks were approximately 33% and 59% of the total N and P sources, respectively, to the inner LCS.

Citation: Lehrter, J. C., D. S. Ko, M. C. Murrell, J. D. Hagy, B. A. Schaeffer, R. M. Greene, R. W. Gould, and B. Penta (2013), Nutrient distributions, transports, and budgets on the inner margin of a river-dominated continental shelf, *J. Geophys. Res. Oceans*, *118*, 4822–4838, doi:10.1002/jgrc.20362.

1. Introduction

[2] The contribution of Mississippi River nutrients to Louisiana continental shelf (LCS) primary production [*Riley*, 1937; *Walsh et al*., 1989; *Lohrenz et al*., 2008] is of interest owing to the productive fisheries of the region and to the linkage of river nutrients to coastal eutrophication and the development of bottom water hypoxia [*Rabalais et al*., 2002; *Bianchi et al*., 2010]. The LCS hypoxic area is among the largest in coastal regions [*Diaz and Rosenberg*, 2008], and variability in the annual areal extent (average from 1985 to present = 15,000 km^2 [*Rabalais et al*., 2002]) covaries with the spring discharge and nutrient concentrations of the Mississippi and Atchafalaya rivers [*Turner et al*., 2006; *Greene et al*., 2009]. The hypoxic area is generally confined to bottom waters (thickness of 1–10 m) of the LCS between the 5 and 30 m isobaths, but has been observed at depths up to 60 m, and occurs annually, generally May to September [*Rabalais et al*., 2002].

[3] The primary source of nutrients to the LCS is the Mississippi-Atchafalaya river basin (MARB) [*Dunn*, 1996], with other, mainly unquantified, inputs from coastal bays, and upwelling of nutrients from waters below the mixed-layer depth off the shelf [*Walsh et al*., 1989; *Sahl et al*., 1993; *Chen et al*., 2000]. Other potential sources of nutrients such as atmospheric loads of nitrogen deposited directly to the shelf waters and groundwater loads are considered small in comparison with the river loads [*Goolsby et al*., 1999; *Rabalais et al*., 2002]. The loads delivered by the Mississippi River and Atchafalaya River both impact the LCS. Generally, the buoyant freshwater plume of the Mississippi River travels westward [*Dinnel and Wiseman*, 1986; *Walker et al*., 2005], which is the direction of the mean current on the inner shelf [*Cochrane and Kelly*, 1986; *Nowlin et al*., 2005], and becomes entrained in the Louisiana coastal current [*Wiseman et al*., 1997]. However, because the Mississippi River discharges to a narrow region of the shelf, seasonal

[1]US EPA, Office of Research and Development, Gulf Breeze, Florida, USA.
[2]Naval Research Laboratory, Stennis Space Center, Mississippi, USA.

Corresponding author: J. C. Lehrter, US EPA, Office of Research and Development, 1 Sabine Island Drive, Gulf Breeze, FL 32561, USA. (lehrter.john@epa.gov)

2169-9275/13/10.1002/jgrc.20362

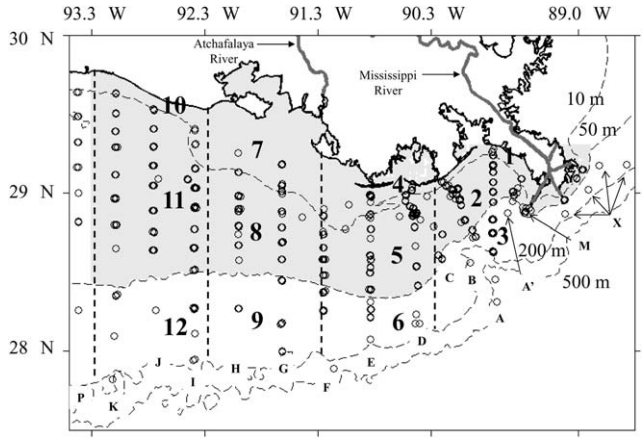

Figure 1. Map of the LCS depicting the sampling locations (open circles) and budget control volume (gray area). The letters denote transects. Regions 1–12, constructed to examine spatial means of nutrients and organic carbon, were bounded by the coast, 10 m, 50 m, and 200 m isobaths and the vertical dashed lines at longitudes 90.3°W, 91.3°W, 92.3°W, and 93.3°W.

changes in wind direction and interactions with Loop Current eddies can promote cross-shelf transport of river water in this region [*Schiller et al*., 2011]. In contrast, the Atchafalaya River discharges where the LCS is broad and the prevailing mean current direction is westward, resulting in along-shelf freshwater transport confined to the inner shelf [*Zhang et al*., 2012].

[4] Relative to freshwater transport, less is known about the transport pathways of nitrogen (N) and phosphorus (P) or about the magnitudes of sources and sinks of inorganic and organic N and P. First order nitrogen budgets have been calculated for the LCS [*Walsh et al*., 1989; *Nixon et al*., 1996]. However, phosphorus budgets have not been calculated, and there is a need for better description of P spatial and temporal patterns in light of its potential role as a limiting nutrient to primary production on this shelf [*Sylvan et al.,* 2006]. For both N and P, the processes regulating the fate of nutrients delivered by the MARB are not sufficiently understood [*Dagg and Breed*, 2003; *Bianchi et al*., 2010].

[5] Based on the mean westward currents on the inner LCS [*Cochrane and Kelly*, 1986; *Nowlin et al*., 2005], it can be inferred that most of the river nutrients follow this transport pathway. Though, modeling and observational studies have also indicated potentially large cross-shelf exchanges of freshwater [*Schiller et al*., 2011; *Zhang et al*., 2012] and nutrients [*Sahl et al*., 1993]. High nutrient uptake rates and high rates of primary production in the Mississippi River plume [*Lohrenz et al*., 1999, 2008] and the correspondence of riverine nutrient loads with surface water autotrophy and bottom water heterotrophy [*Justić et al*., 1997] indicate rapid removal of inorganic nutrients and production of organic matter near the plumes. However, other continental shelf systems with terrestrial margins dominated by coastal marshes may be net heterotrophic as a result of marsh organic matter exports [*Cai et al*., 2003], and for the LCS, it has been estimated that riverine and marsh-derived organic matter could contribute significantly to metabolism [*Bianchi et al*., 2011]. There is still much unknown about the processes governing nutrient and organic carbon dynamics on the LCS, and, compared to well-studied estuaries, relatively little data are available to test hypotheses and models.

[6] In this study, nutrient mass balance budgets were constructed for the LCS from observations of river nutrient loads, nutrient concentrations on the shelf, and current velocities obtained from a three-dimensional (3-D) hydrodynamic model (the Navy Coastal Ocean Model). The budget terms were used to examine the processes underlying the distribution, transport, and fate of nutrients on the LCS. Currently, there is work underway to develop coupled 3-D hydrodynamic-eutrophication models of the LCS [*Justić et al*., 2007; *Fennel et al*., 2011, 2013] to inform nutrient management actions in the MARB that could reduce the hypoxic area on the shelf. This study constrains the physical and biological process rates controlling the transport and fate of nutrients and organic matter on the LCS, and allowed for a quantitative examination of these processes relative to nutrient loads from the MARB.

2. Methods

2.1. Nutrient and Organic Carbon Observations

[7] Nutrient and organic carbon concentrations were measured on the LCS (Figure 1) during 12 cruises from 2002 to 2007 (Table 1). At each station, vertical profile data were collected with a conductivity, temperature, and depth (CTD) instrument (Sea-Bird 911, Sea-Bird Electronics, Bellvue, WA), which measured salinity, temperature, depth, and dissolved oxygen. Dissolved oxygen was measured with a membrane sensor (Sea-Bird Electronics 43 Clark polarographic sensor), and O_2 concentrations obtained by sensor were validated against O_2 measurements via Winkler titrations obtained at discrete depths [*Murrell and Lehrter*, 2011]. Pycnocline depths were estimated at each station as the depth of the maximum Brunt-Väisälä frequency determined from vertical profiles of density, calculated from temperature and salinity profiles [*Pond and Pickard*, 1983].

[8] Water samples were collected at multiple discrete depths. At a minimum, a sample was collected approximately 1 m below the surface and approximately 2 m above the bottom using vertically oriented 10 L Niskin bottles. Water samples were processed within an hour of sampling by filtration through ashed (450°C for 90 min) glass fiber filters (Whatman GF/F, nominal pore size = 0.7 μm) to prepare samples for dissolved and particulate inorganic and organic nitrogen, phosphorus, and carbon. With the exception of ammonium (NH_4^+), which was analyzed shipboard during 2006 and 2007, samples were frozen at −70°C until analysis.

[9] Nitrate+nitrite ($NO_3^-+NO_2^-$), nitrite (NO_2^-), orthophosphate (PO_4^{3-}), and silica (SiO_2) were analyzed by wet chemistry methods [*APHA*, 1989] with a continuous flow analyzer (Astoria-Pacific International). Ammonium (NH_4^+) was measured fluorometrically (Turner Designs 700 fluorometer) [*Holmes et al*., 1999]. Total dissolved nitrogen (TDN) was analyzed by two different methods. TDN samples collected from 2002 to 2006 were analyzed

Table 1. Summary of Shelfwide Cruises

Cruise Dates	CTD Stations	Nutrient Stations	Nutrient Samples	Depth Range (m)	Salinity Range	Transects Occupied
3–12 Dec. 2002	35	21	77	7.6–320	24.9–36.5	A, D, F, H, J
18–27 Mar. 2003	65	24	116	7.4–549	9.7–36.5	A, C, D, F, G, H, I, J, P
12–20 Jun. 2003	49	26	89	7.7–171	0.2–36.3	A, C, D, E, F, H, M
6–16 Nov. 2003	66	43	128	6.8–175	1.4–36.6	A, B, C, D, E, F, G, H, J, M
2–6 Apr. 2004	20	18	36	6.4–51	0.2–36.5	A, B, C, D, E, F
22–30 Mar. 2005	62	38	139	6.8–345	0.2–36.6	A, B, C, D, F, H, J, M
29 Sep–7 Oct. 2005	0[a]	47	130	5.4–305	2.6–36.6	A, B, C, D, E, F, G, H, J, X
13–17 Apr. 2006	63	42	181	6.5–67	3.1–36.5	A, A', B, C, D, E, F, G, H, J, M
6–11 Jun. 2006	82	73	396	7.3–134	1.1–37.1	A, B, C, D, E, F, G, H, I, J, K, M, X
6–11 Sep. 2006	90	82	423	6.6–110	6.6–36.6	A, A', B, C, D, E, F, G, H, I, J, K, M, X
2–7 May 2007	88	88	377	5.1–116	0.9–36.7	A, B, C, D, E, F, G, H, I, J, K, M, X
19–24 Aug. 2007	86	78	331	6.0–108	5.4–36.6	A, B, C, D, E, F, G, H, I, J, K, M, X
Total	706	580	2423			

[a]Discrete surface and bottom layer hydrography and nutrient samples were collected during this cruise.

colorimetrically [*Menzel*, 1965] following persulfate oxidation on a spectrophotometer (Shimadzu UV1700 dual beam). From 2006 to 2007, TDN samples were analyzed following high-temperature catalytic oxidation [*Sharp*, 1973] on a chemiluminescent detector (Shimadzu TOC-VCSN analyzer). TDN samples collected on four shelfwide cruises were analyzed using both methods. A regression comparison of the results from the two methods indicated close agreement (slope = 0.96, $R^2 = 0.89$, n = 959). Dissolved organic nitrogen was calculated as the difference of TDN and dissolved inorganic nitrogen (DIN), which is the sum of $NO_3^- + NO_2^- + NH_4^+$. Particulate nitrogen (PN) and particulate carbon (PC) were measured on an elemental analyzer (Carlo-Erba) following high-temperature catalytic oxidation [*Sharp*, 1974].

[10] Total dissolved phosphorus (TDP) and particulate phosphorus (PP) were measured colorimetrically on a spectrophotometer, following persulfate oxidation [*Menzel*, 1965]. Dissolved organic phosphorus (DOP) was calculated as the difference of TDP and dissolved inorganic phosphorus (DIP), i.e., measured PO_4^{3-}. Dissolved organic carbon (DOC) samples were collected on six cruises from September 2005 to August 2007. DOC was measured (Shimdazu TOC-VCSN analyzer) following acidification to pH = 2 with 2 *N* HCl and high-temperature oxidation [*Sharp*, 1973].

[11] Mean method detection limits (MDL) for $NO_3^- + NO_2^-$, NO_2^-, NH_4^+, TDN, and PN were 0.27, 0.026, 0.089, 0.65, and 0.48 mmol N m^{-3}, respectively; for PO_4^{3-}, TDP, and PP were 0.035, 0.041, and 0.065 mmol P m^{-3}, respectively; and for DOC and PC were 3.07 and 3.54 mmol C m^{-3}, respectively. Samples for $NO_3^- + NO_2^-$ were observed to be below MDL 27% of the time, and for PO_4^{3-} were below MDL 2% of the time. Samples below MDL occurred primarily in surface waters at offshore stations (i.e., locations with depths > 50 m). Lacking further information about the distribution of values below the MDL, the values generated by the analytical methods were reported, with the exception of negative values that were set to zero. Field process blanks were also collected and analyzed to assess the effects of sample processing, storage, and analysis. Field blanks were obtained at approximately every 10th station by filtering 250 mL of deionized water through ashed GF/F filters using the same processing procedures as for samples. Filter pad and filtrate blanks were then stored with samples until analysis. Average concentrations of field blanks were less than the method detection limits.

2.2. Mississippi and Atchafalaya River Discharge, Nutrients, and Organic Carbon

[12] Mississippi River and Atchafalaya River daily discharge records were downloaded from the Tarbert Landing gauge site on the lower Mississippi River [USACOE gauge 01100, http://www.mvn.usace.army.mil/cgi-bin/wcmanual.pl?01100] and the Simmesport site on the Atchafalaya River [USACOE gauge 03045, http://www.mvn.usace.army.mil/cgi-bin/watercontrol.pl?03045]. River nutrients and organic matter data were obtained from the USGS National Water Information System [NWIS, http://waterdata.usgs.gov/nwis] for a site on the lower Mississippi River at St. Francisville, LA (USGS Site 07373420), and for a site on the Atchafalaya River at Melville, LA (USGS Site 07381495). River water quality data (with USGS parameter codes and abbreviations used herein) obtained for the study period included filtered ammonium (P00608, NH_4^+), filtered total Kjeldal nitrogen (P00623, TKN), unfiltered TKN (P00625), filtered nitrate plus nitrite (P00631, NO_3^-), filtered orthophosphate (P00671, PO_4^{3-}), filtered phosphorus (P00665), unfiltered phosphorus (P00666, TP), filtered organic carbon (P00681, DOC), and suspended sediment organic carbon (P00689, PC). Dissolved organic nitrogen (DON) was calculated as the difference of filtered TKN and filtered NH_4^+. Particulate nitrogen (PN) was calculated as the difference between unfiltered and filtered TKN. Total nitrogen (TN) was calculated as the sum of NO_3^-, NH_4^+, DON, and PN. Dissolved organic phosphorus (DOP) was calculated as the difference of filtered phosphorus and filtered orthophosphate. Particulate phosphorus (PP) was calculated as the difference of unfiltered and filtered phosphorus.

[13] Instantaneous riverine and organic matter loads (mmol s^{-1}) were calculated as the products of daily discharge and the USGS observations during 2002 to 2007. Mean seasonal, nonsummer (n = 59) and summer (n = 28),

and mean study period loads (n = 87) were calculated from the instantaneous loads for comparison to shelf transport rates and input to budgeting calculations (described below).

2.3. Hydrodynamic Model

[14] The Navy Coastal Ocean Model (NCOM) [*Martin*, 2000] was implemented on a 3-D grid constructed for the LCS to model the hydrodynamics from 2002 to 2007. The model domain, hereafter referred to as NCOM-LCS, has the spatial extent of Figure 1, a horizontal spatial resolution of 1.9 km, and up to 34 hybrid vertical layers. Depths shallower than 100 m were represented by 20 equally spaced terrain following sigma layers. The discharge time series for the Mississippi and Atchafalaya rivers, obtained from the USACOE as described above, and discharges from other smaller rivers, obtained from USGS, were used as the freshwater inputs (91 discharges in total) to the model. NCOM-LCS boundary conditions for the eastern, southern, and western open ocean boundaries were provided by a regional implementation of NCOM covering the Gulf of Mexico and Caribbean Sea, the Intra-America Seas Nowcast/Forecast System (IASNFS) [*Ko et al*., 2003]. To improve these boundary conditions, the IASNFS model was updated to use daily river discharge observations, instead of monthly discharge climatologies, for 103 rivers discharging to the IASNFS model domain. Atmospheric forcings were described by *Ko et al*. [2008] and consisted of three hourly, 9 km scale estimates of air pressure, wind stress, solar radiation, and temperature from the Navy's Coupled Ocean/Atmosphere Mesoscale Prediction System (COAMPS). COAMPS winds were increased by 5% to account for an observed underprediction bias as compared to observations (described below in section 3.2)

[15] For typical NCOM runs, solar shortwave transparency in the ocean is parameterized in COAMPS as a uniform Jerlov oligotrophic oceanic water Type IA [*Jerlov*, 1976]. This approach ignores potential variability in water-column absorption of solar radiation across the model domain, which can lead to significant errors in radiation penetration and ocean/atmosphere thermal energy exchange [*Hetland and DiMarco*, 2012], particularly in coastal waters with complex optical characteristics [*Jolliff et al*., 2012]. To account for spatial variability in water-column absorption properties (e.g., higher absorption in plume and inshore regions related to higher concentrations of chlorophyll *a*, chromophoric dissolved organic matter, and suspended particulate matter), NCOM-LCS was modified to use estimated light attenuation from MODIS-Aqua. Monthly MODIS-Aqua composite images of the diffuse attenuation coefficient at 488 nm ($K_d(488)$) were created using the *Lee et al*. [2005] K_d algorithm. $K_d(488)$ was subsequently converted to K_{PAR} based on empirical algorithms for the LCS [*Schaeffer et al*., 2012] and used to absorb solar radiation in the water column of the model.

[16] The surface salinity flux (the net balance of precipitation and evaporation) to the model was estimated using rainfall rates for the model domain obtained from the Tropical Rainfall Measurement Mission's (TRMM) Microwave Imager (TMI) on the TRMM satellite. Gridded, monthly rainfall accumulation data (3B43 V7) were downloaded from the TRMM Online Visualization and Analysis System (TOVAS) web site (http://disc2.nascom.nasa.gov/Giovanni/tovas/). The satellite data products provided spatially improved estimates of surface layer heat and freshwater boundary forcing and accounted for known biases in the model.

2.4. Spatial Distribution of Freshwater, Nutrient, and Organic Carbon and Calculation of Transport Rates and Budgets

[17] The LCS was delineated into 12 regions to examine the spatial distributions of freshwater, nutrients, and organic carbon (Figure 1). The regionalization scheme was adopted to examine cross-shelf gradients in three discrete regions; nearshore (<10 m depth), midshelf (10–50 m depth), and outer shelf (>50 m depth), and to examine along-shelf (east to west) gradients originating at the birdsfoot delta of the lower Mississippi River and extending west of the Atchafalaya River. Areally, weighted means and standard errors were calculated from the stations occurring within each region. Budgets (described below) were calculated for the inner shelf regions (<50 m depth). The east-west regional boundaries were spaced at 1° longitude and selected to describe the inner shelf regions of the LCS immediately adjacent to river discharges (regions 1, 2, 7, and 8) and the inner shelf regions more removed from riverine influence (regions 4, 5, 10, and 11). The 50 m isobath was selected as the offshore boundary of the budget domain because this is the approximate location of the current speed isotach = 0. Inshore of 50 m the prevailing current is westward and offshore the prevailing current is eastward [*Nowlin et al*., 2005].

[18] Mean budgets of N and P were calculated as a mass balance of the transport and reaction terms at assumed steady state

$$C_{east} + C_{west} + C_{south} + C_{rivers} + R_C = 0, \quad (1)$$

where C_{east}, C_{west}, and C_{south} were the transport rates at the east, west, and south boundary faces, respectively, and C_{rivers} were the river constituent loads. R_C was the net nonconservative flux (mmol s^{-1}) for constituent C. All the terms except for R_C in equation (1) may be directly calculated and rearranging to solve for R_C yields

$$R_C = -(C_{east} + C_{west} + C_{south} + C_{rivers}). \quad (2)$$

[19] Thus, R_C is taken to be the net source/sink ± propagated error. Transports at the east, west, and south boundaries were calculated as the products of current velocity and concentration at the boundary face. Owing to the large temporal and spatial scale of the budgeting analysis, advection was assumed to be the dominant transport and dispersion was assumed equal to zero. C_{east} and C_{west} were calculated as

$$C_{east} \text{ or } C_{west} = \sum u_{S\_ij} C_{x\_S\_ij} x_{ij} z_{S\_ij} + \sum u_{B\_ij} C_{x\_B\_ij} x_{ij} z_{B\_ij} \quad (3)$$

and C_{south} was calculated as

$$C_{south} = \sum v_{S\_ij} C_{y\_S\_ij} y_{ij} z_{B\_ij} + \sum v_{B\_ij} C_{y\_B\_ij} y_{ij} z_{B\_ij} \quad (4)$$

where u was the mean monthly current velocity (m s^{-1}) in the x (east-west) direction and v was the mean monthly

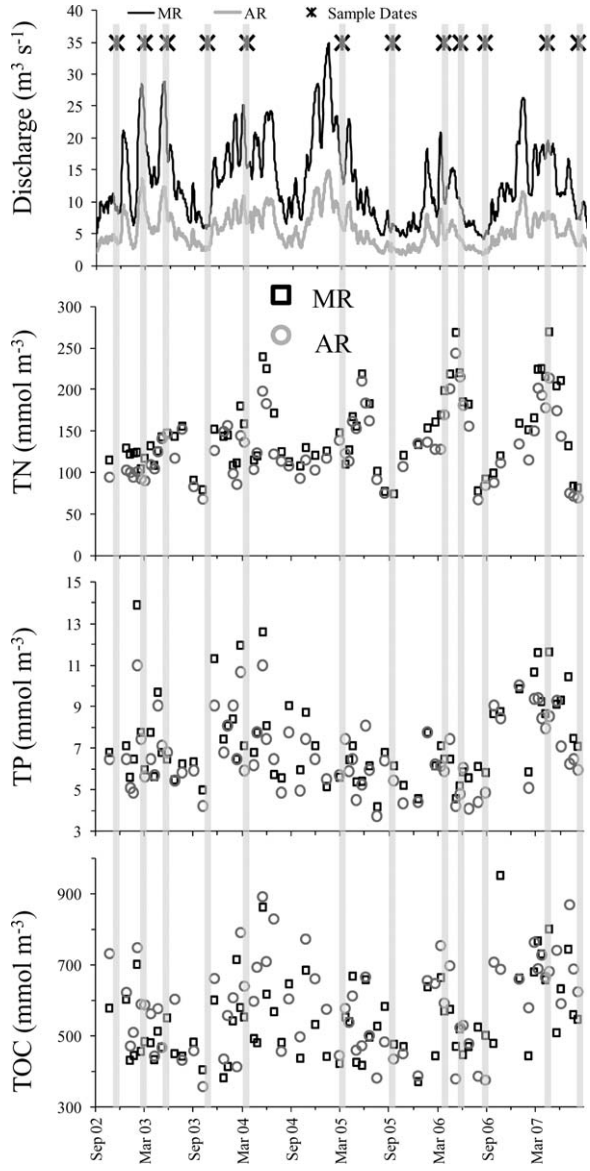

Figure 2. Time series of Mississippi and Atchafalaya river (MR and AR) discharge and discrete measures of TN, TP, and TOC from 2002 to 2007 for the MR (open squares) and AR (open circles).

current velocity in the *y* (north-south) direction. A negative value for *u* indicates a current directed toward the west and a negative value for *v* indicates a current directed toward the south. C_x and C_y were the average surface (S) and bottom (B) concentrations, by cruise, interpolated to the east/west and south boundary faces, respectively. *S_ij* were the surface *ij* cells comprising the boundary face and *B_ij* were the bottom *ij* cells of the boundary face. The cross-sectional area of each *ij* face was calculated as the product of *x* and *z* or *y* and *z*, where *x* and *y* were the grid cell length (1.9 km) and z_{S_ij} for surface cells was the pycnocline depth and z_{B_ij} for bottom cells equaled the total depth – pycnocline depth. Horizontal interpolations of constituent concentrations to the boundary faces were conducted in MATLAB (Mathworks; Natick, MA) where average surface and bottom layer constituent concentrations from each station, were interpolated to the *ij* grid. Average surface and bottom concentrations at each station were calculated from samples above and below the main pycnocline depths. In most cases, surface and bottom layer nutrient and organic carbon concentrations at a station were represented by a single measure. In these cases, it was assumed that the single observed concentration was representative of the layer. Inspection of multipoint profiles of nutrients and organic carbon measurements, based on up to 20 vertical discrete measures throughout the water column (data not shown), suggested large vertical concentrations gradients, when present, occurred near the pycnocline and near (<1 m) the bottom. The single-point assumption for the LCS was previously validated against multiple-point measures of respiration rates in a layer [*Murrell and Lehrter*, 2011].

[20] To calculate freshwater flux, the fraction of freshwater (F_{fw}) at each boundary face was calculated from salinity observations as

$$F_{fw} = \frac{S_{\max} - S}{S_{\max}} \tag{5}$$

where $S_{max} = 37$, the maximum salinity on the shelf, and *S* was the vertically weighted average salinity at the interpolated boundary face. Freshwater transport rates ($m^3\ s^{-1}$) across the boundary faces were then calculated from equations (3) and (4), substituting F_{fw} for *C*. Filling and flushing times for the inner LCS budget control volume (Figure 1) were also calculated for nutrients, organic carbon, and freshwater. For nutrients and organic carbon constituents, the filling times were based on the loading rates from the MARB and were calculated as the (mass of constituent in the control volume)/(MARB load). Flushing rates were calculated (mass of constituent in the control volume)/(sum of transport rates out of the control volume). Standard errors (SE) were propagated through equation (2) using Gaussian error propagation [e.g., *Lehrter and Cebrian*, 2010] to provide an SE for each R_C, and filling and flushing time calculation.

3. Results

3.1. Observed Spatial and Temporal Patterns of Salinity, Nutrients, and Organic Carbon

[21] The relative fraction of MARB discharge distributed through the lower Mississippi and Atchafalaya rivers is controlled by the U.S. Army Corps of Engineers (at the Old River Control Structure), and, thus during the study period, the Mississippi River discharge (mean ± SE = 13,423 ± 143 $m^3\ s^{-1}$) represented a nearly constant 70% of the combined Mississippi and Atchfalaya freshwater discharge (Figure 2). Observed spatial patterns of salinity and nutrients reflected proximity to the Mississippi and Atchafalaya rivers (Figure 3), where shelf regions in the plume and near the coast had lowest salinity (<25, Table 2) and regions away from the plumes and coast had increasing salinity and diminishing nutrients and organic carbon.

[22] By season, observed DIN and DIP concentrations varied with largest concentrations generally occurring during the spring in the surface waters of nearshore (<10 m depth) sites and near the inputs of the Mississippi and Atchafalaya rivers (data not shown). Regionally, DIN

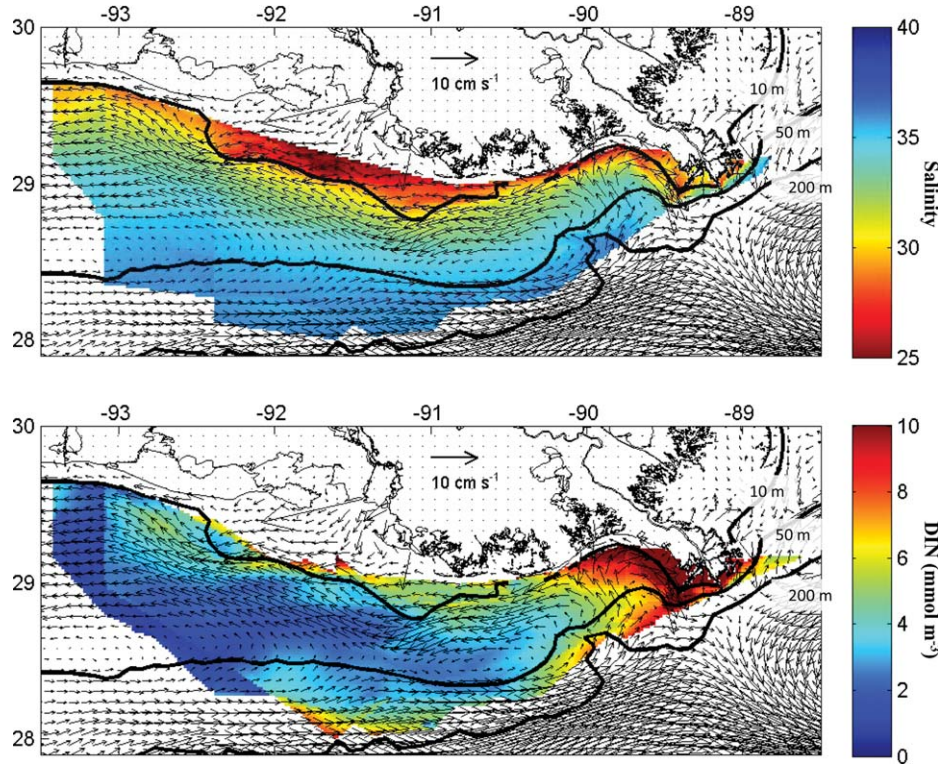

Figure 3. Interpolated mean salinity (upper) and mean DIN (lower) for the whole water-column interpolated to the model grid and overlaid with the mean modeled currents (whole water-column) for the study period (December 2002 to August 2007).

concentrations (Table 3) were largest inshore, <10 m depth, and varied inversely with salinity (Figure 4). Elevated DIN was also observed at depths > 100 m where NO_3^- beneath the pycnocline was >20 mmol m^{-3} (data not shown). This deeper NO_3^- pool resulted in larger mean concentrations for some regions of the outer shelf (>50 m depth) than for adjacent midshelf (10–50 m depth range) regions (Table 3). DON comprised a significant fraction of the TN on the shelf with regional means ranging from 5.2 to 15.9 mmol m^{-3} in surface waters. For the inner LCS (<50 m depth; regions 1, 2, 4, 5, 7, 8, 10, and 11; Figure 1), the spatially weighted average TN concentration was 24.1 ± 3.5 mmol m^{-3}, which was five- to sixfold lower than the TN concentration in the Mississippi and Atchafalaya rivers over the study (146 ± 4.8 and 128 ± 4.3 mmol m^{-3}, respectively). On average, the TN pool was composed of 31% DIN, 37% DON, and 32% PN, whereas DIN (mainly NO_3^-) was the dominant form in the rivers, being on average 71% and 65% of the TN in the Mississippi and Atchafalaya, respectively.

Table 2. Physical Dimensions and Conservative Properties for the Regions Defined by Figure 1[a]

Region	Longitude	Depth Range (m)	Z_{pycno} (m)	A (10^9 m^2)	V_{Surf} (10^9 m^3)	V_{Bott} (10^9 m^3)	S_{surf}	S_{Bott}	F_{FW_Surf}	F_{FW_Bott}
1	<90.3°W	<10	4.4 (0.14)	5.6	23.5	2.4	24.9 (0.51)	30.7 (0.48)	0.33 (0.011)	0.17 (0.006)
2		10–50	8.7 (0.07)	6.6	42.1	74.8	26.7 (0.13)	34.8 (0.04)	0.28 (0.004)	0.06 (0.000)
3		50–200	14.2 (0.26)	6.6	76.4	356	33.1 (0.21)	36.1 (0.01)	0.11 (0.002)	0.02 (0.000)
4	90.3° to 91.3°W	<10	5.0 (0.16)	3.3	7.8	4.4	27.4 (0.24)	30.2 (0.25)	0.26 (0.004)	0.19 (0.003)
5		10–50	11.5 (0.09)	5.6	62.1	92.3	31.0 (0.05)	35.2 (0.02)	0.16 (0.001)	0.05 (0.000)
6		50–200	33.8 (0.59)	3.8	101	251	34.8 (0.13)	36.2 (0.02)	0.06 (0.001)	0.02 (0.000)
7	91.3° to 92.3°W	<10	3.6 (0.16)	6.1	20.0	11.3	26.6 (0.44)	28.7 (0.55)	0.28 (0.008)	0.22 (0.009)
8		10–50	14.1 (0.22)	6.3	72.8	63.4	32.8 (0.08)	35.3 (0.04)	0.11 (0.001)	0.05 (0.000)
9		50–200	35.1 (0.36)	6.2	169	301	35.7 (0.03)	36.2 (0.01)	0.04 (0.000)	0.02 (0.000)
10	>92.3°W	<10	5.3 (0.14)	1.5	15.5	6.1	21.7 (0.97)	21.7 (1.14)	0.41 (0.026)	0.41 (0.030)
11		10–50 m	5.4 (0.10)	11.7	121	113	33.3 (0.03)	35.0 (0.02)	0.10 (0.000)	0.05 (0.000)
12		50–200	33.5 (0.61)	6.7	199	354	36.0 (0.02)	36.2 (0.01)	0.03 (0.000)	0.02 (0.000)

[a]For each region, mean pycnocline depth (Z_{pycno}), surface area (A) and surface (Surf) and bottom (Bott) layer volume (V), mean salinity (S), and mean fraction freshwater (F_{FW}) are shown. Standard error of the mean is shown in parentheses. Errors shown as 0.000 are <0.0005. Errors in A and V were negligible. $V_{Surf} \neq A \times Z_{pycno}$, in this table as volumes were calculated as the sum of the surface or bottom ij volumes per region, where the surface and bottom of each ij cell was defined from observed pycnocline depths interpolated to the *ij* NCOM-LCS model grid.

Table 3. Nonconservative Dissolved Constituents for the Regions Defined by Figure 1[a]

Region	Longitude	Depth Range (m)	DIN_{Surf}	DIN_{Bott}	DON_{Surf}	DON_{Bott}	DIP_{Surf}	DIP_{Bott}	DOP_{Surf}	DOP_{Bott}	DOC_{Surf}	DOC_{Bott}
1	<90.3°W	<10	13.0 (3.5)	11.0 (3.2)	10.2 (1.3)	8.7 (1.6)	0.54 (0.07)	0.52 (0.09)	0.57 (0.26)	0.24 (0.03)	189 (20)	136 (13)
2		10–50	11.3 (1.4)	6.0(0.4)	11.2 (0.8)	6.9 (0.3)	0.39 (0.03)	0.44 (0.02)	0.25 (0.01)	0.21 (0.01)	174 (6)	103 (5)
3		50–200	7.2 (2.7)	5.5 (0.6)	7.9 (1.0)	5.4 (0.4)	0.23 (0.04)	0.38 (0.03)	0.17 (0.02)	0.15 (0.01)	166 (11)	119 (11)
4	90.3° to 91.3°W	<10	10.4 (0.9)	11.2 (0.8)	12.1 (1.0)	10.2 (0.4)	0.22 (0.02)	0.54 (0.08)	0.17 (0.01)	0.12 (0.01)	230 (11)	198 (11)
5		10–50	5.2 (0.4)	6.2 (0.3)	9.2 (0.3)	7.6 (0.3)	0.17 (0.01)	0.72 (0.05)	0.21 (0.01)	0.19 (0.01)	159 (5)	131 (7)
6		50–200	2.4 (1.0)	5.6 (1.3)	5.2 (0.7)	5.4 (1.2)	0.16 (0.04)	0.32 (0.04)	0.13 (0.02)	0.19 (0.02)	129 (12)	84 (10)
7	91.3° to 92.3°W	<10	12.5 (2.9)	16.7 (4.7)	15.2 (1.3)	12.7 (1.2)	0.31 (0.05)	0.36 (0.07)	0.35 (0.07)	0.40 (0.09)	241 (27)	286 (50)
8		10–50	2.3 (0.4)	3.3 (0.3)	10.1 (0.5)	8.6 (0.5)	0.17 (0.02)	0.27 (0.03)	0.18 (0.01)	0.23 (0.01)	149 (8)	116 (8)
9		50–200	1.7 (0.5)	5.1 (0.7)	8.3 (0.8)	9.4 (0.8)	0.17 (0.02)	0.32 (0.03)	0.15 (0.02)	0.22 (0.02)	86 (5)	77 (5)
10	>92.3°W	<10	26.1 (3.8)	28.2 (4.0)	15.3 (1.4)	15.9 (2.0)	1.17 (0.13)	1.30 (0.14)	0.50 (0.06)	0.63 (0.10)	331 (18)	353 (22)
11		10–50	1.5 (0.2)	1.9 (0.2)	8.8 (0.3)	7.3 (0.3)	0.15 (0.01)	0.21 (0.01)	0.16 (0.01)	0.16 (0.01)	127 (2)	106 (2)
12		50–200	2.0 (1.1)	4.3 (1.7)	12.2 (1.9)	12.1 (2.9)	0.13 (0.02)	0.25 (0.04)	0.18 (0.03)	0.15 (0.03)	115 (21)	86 (15)

[a]For each region, mean DIN, DON, DIP, DOP, and DOC concentrations for surface (Surf) and bottom (Bott) layers. Standard error of the mean is shown in parentheses. Concentration units are mmol m^{-3}.

[23] As with DIN, average regional DIP concentrations (Table 3) were highest in regions with salinity <25 and depths <10 m. The spatially weighted mean for the inner LCS (defined above) was 1.01 ± 0.17 mmol m^{-3} and comprised mainly of PP (47%) and DIP (33%). Mean TP in the Mississippi and Atchafalaya rivers was 7.3 ± 0.23 and 6.7 ± 0.20 mmol m^{-3}, respectively, with PP being 67% of the TP.

[24] Mixing diagrams constructed for each cruise indicated uptake of inorganic nutrients and production of organic N and P at salinity between 10 and 30, with maximal production of organic matter occurring at salinity of 20–25. As an example of a seasonal progression from spring to late summer (April, June, and September 2006), the mixing diagrams in Figure 4 have similar overall patterns but the magnitudes of concentrations differ. The June 2006 sampling followed an annual peak in river discharge and nutrient concentrations (Figure 2). During the June to September 2006 period, bottom layer O_2 concentrations were observed to decrease and DIP concentrations increased (Figure 5), presumably due to benthic remineralization and sediment release of phosphate under reducing conditions.

[25] The mixing diagrams for DOC and PC were similar to those for organic nutrients, and had elevated river concentrations and a smaller, secondary peak in concentrations occurring in a salinity range of 20–30 (Figure 4). DOC data were only collected on the 2006 and 2007 cruises ($n = 5$ cruises), but the mixing diagram patterns and the seasonal variations in regional means indicated that the DOC concentrations on the shelf were higher in April of 2006 (Figure 4) and 2007 (data not shown) than for the summer months in the same years. Mean regional DOC (Table 3) and PC (data not shown) concentrations were largest in the <10 m regions where average DOC was 167 ± 5.6 and PC was 53.4 ± 13.6 mmol m^{-3}. Stations with depths of 10–50 m had average DOC of 127 ± 4.5 and PC of 80.4 ± 19.1 mmol m^{-3}. The spatially weighted average TOC for the inner LCS (defined above) was 216 ± 28.5 mmol m^{-3}, with DOC comprising 68% of the TOC. In comparison, the average TOC concentrations in the Mississippi and Atchafalaya rivers were 550 ± 12.1 and 595 ± 14.5 mmol m^{-3}, respectively, with DOC being 54% of the TOC in the Mississippi River and 62% in the Atchafalaya River.

[26] PC, PN, and PP were significantly correlated ($p < 0.05$, Figure 6) and ratios were similar to Redfield, with PC:PN (C:N = 7.3 ± 0.25), PC:PP (C:P = 110 ± 3.8), and PN:PP (N:P = 17 ± 0.72). DOC, DON, and DOP were also significantly correlated ($p < 0.05$, Figure 6), but ratios were much larger than Redfield, with DOC:DON, DOC:DOP, and DON:DOP estimated to be 19 ± 1.3, 834 ± 52.5, and 88 ± 3.8, respectively.

3.2. Hydrodynamic Model

[27] Owing to the importance of wind pattern forcing as a control of LCS low frequency circulation [*Cochrane and Kelly*, 1986], the wind vectors produced by COAMPS were compared with observed wind vectors at the BURL1 sea buoy (NOAA NDBC, latitude = 28.905°N, longitude = 89.428°W). Comparison of mean daily and monthly winds calculated from COAMPS and from the BURL1 data indicated that COAMPS accurately reproduced the

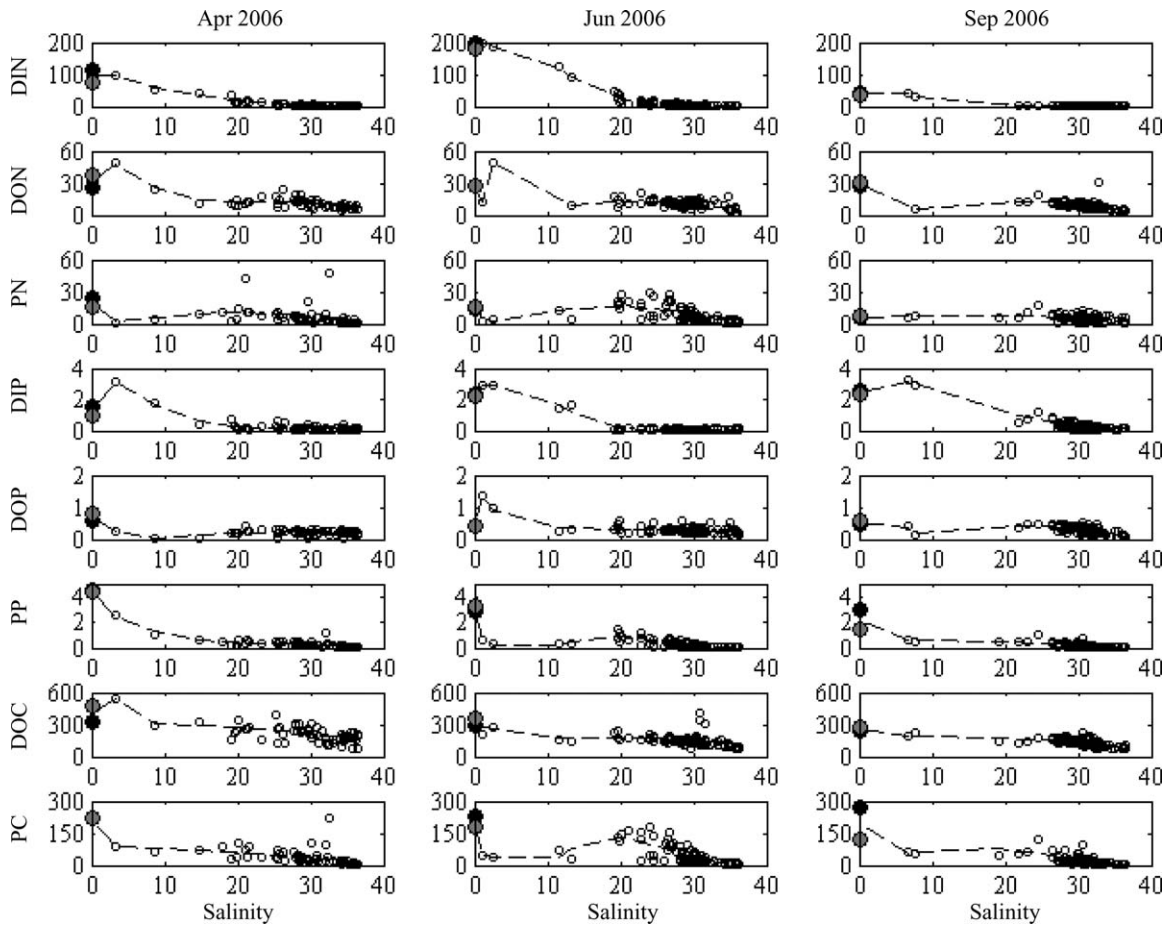

Figure 4. Constituent-salinity plots (i.e., mixing diagrams) from April, June, and September 2006 (columns of subplots). Constituents plotted were DIN, DON, PN, DIP, DOP, PP, DOC, and PC. The dashed line is a stepwise linear regression fit of the constituents regressed against the salinity (S) variables of S, S–2, and exp(−S). The large symbols at zero salinity represent the mean Mississippi River (solid black circle) and Atchafalaya River (solid gray circle) end-member concentrations for the month preceding the shelf observations.

observed wind vectors ($R^2 = 0.87$ and 0.91 for daily and monthly means, respectively, Figure 7), but with a slight underprediction bias (5%, Figure 7). The NCOM-LCS mean inner shelf circulation pattern (Figure 3, mean currents from 2002 to 2007) reflected the local wind forcing, which resulted in a mean westward current of $u = -2.2 \pm 0.03$ cm s^{-1}. At depths between 50 and 200 m, the mean modeled current was larger and eastward ($u = 4.6 \pm 0.04$ cm s^{-1}). Mean modeled cross-shelf current velocities at the 50 m isobath were directed onshore ($v = 0.69 \pm 0.04$ cm s^{-1}), but varied spatially with $v = 1.8 \pm 0.11$ cm s^{-1} east of longitude 90.3°W and $v = 0.24 \pm 0.01$ cm s^{-1} west of longitude 90.3°W. During summer, the modeled current velocities were relaxed and produced some eastward currents on the inner shelf (Figure 5).

[28] As a further check on the accuracy of modeled circulation and mixing the NCOM-LCS derived salinity (S), temperature (T), and density (sigma-t) were compared to observed values. Model-data (2002–2007) comparisons were conducted at a point scale (n = 31,527 discrete hydrographic observations) and at a transect scale (n = 120 transects; transects shown in Figure 1), as this scale was spatially similar to the scale of transport and budgeting calculations. Generally, the model reproduced the observed horizontal and vertical variation in density (sigma-t), salinity, and temperature (Figure 8). Three model metrics [*Lehmann et al.*, 2009] were calculated to assess model agreement with observations and skill at prediction; bias, root-mean-square error (RMSE), and model efficiency (ME). Bias was calculated as the mean residual of modeled and observed values

$$Bias = \frac{1}{n}\sum (M - O), \tag{6}$$

where O was an observed value and M the modeled value. Model agreement with observed values was calculated as the RMSE

$$RMSE = \sqrt{\frac{\sum (O - M)^2}{n}}. \tag{7}$$

[29] The ME evaluates the residuals of observed and modeled values in relation to the observed sum of squares

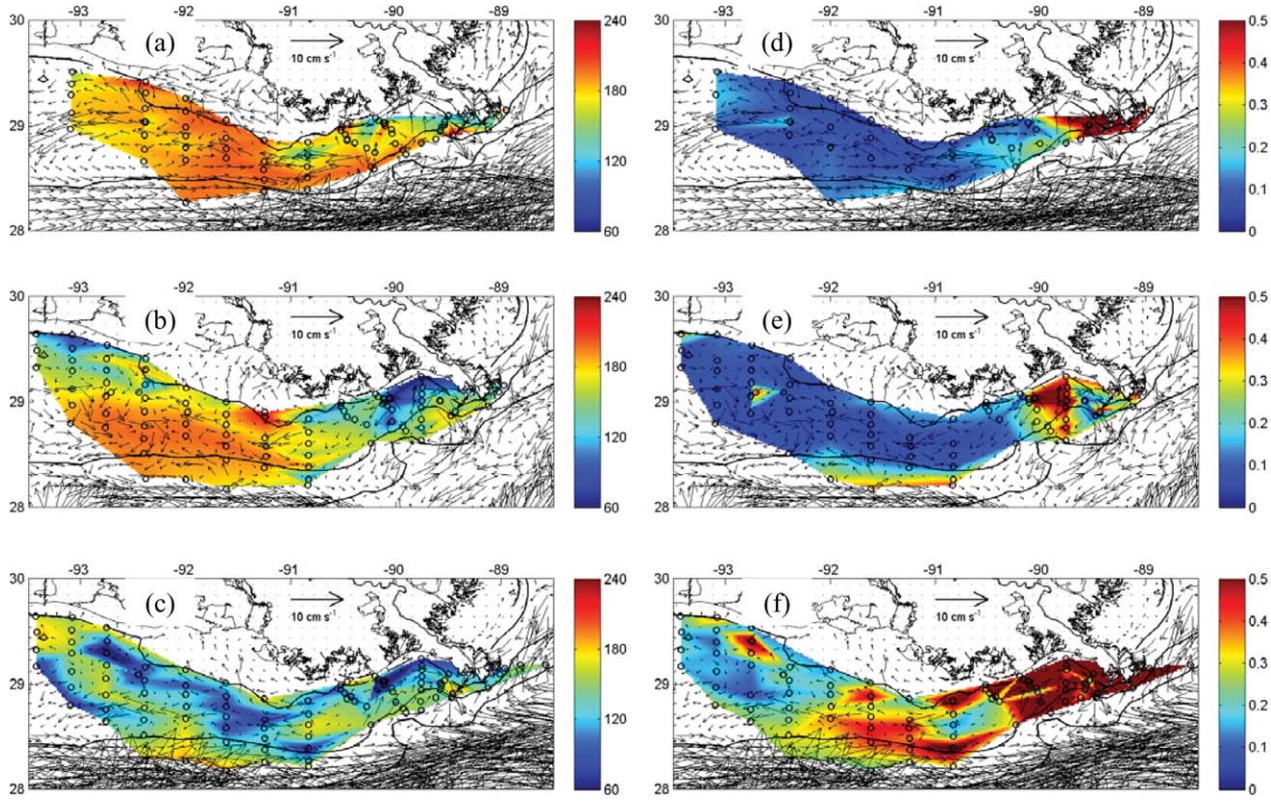

Figure 5. Seasonal changes in bottom-water O_2 and DIP concentrations (mmol m^{-3}). Bottom-water O_2 concentrations are shown for (a) April, (b) June, and (c) September 2006 and bottom-water DIP concentrations are shown for the same months; (d) April, (e) June, and (f) September 2006. Surface layer monthly mean current vectors (cm s^{-1}) are shown as arrows and sampling stations are shown as open black circles. The 10, 50, and 200 m isobaths are shown as black lines.

$$ME = 1 - \frac{\sum (O - M)^2}{\sum (O - \overline{O})^2}. \quad (8)$$

[30] An ME = 1 indicates a perfect correspondence between observed and modeled values, an ME > 0 indicates the model is a better predictor than the mean climatology ($\overline{O}$), and an ME < 0 indicates the climatology is a better predictor than the model. The skill metrics calculated indicated good model agreement and skill at the point scale (n = 31,527; Salinity: bias = −0.41, RMSE = 1.8, ME = 0.64; Temperature: bias = 0.06, RMSE = 0.92, ME = 0.94; sigma-t: bias = −0.32, RMSE = 1.4, ME = 0.74), and better agreement at the transect level (Figure 9) due to averaging. In sum, the modeled patterns were in good agreement with the observations, indicating that the transport processes regulating the distributions of conservative properties were accurately represented in the model. The only model results used further in this study were the mean monthly u and v that were used to calculate along- and cross-shelf constituent transports.

3.4. Budget Domain and Freshwater Transport

[31] To simplify the reporting of budget results, we aggregated the inner LCS regions (Figure 1; regions 1, 2, 4, 5, 7, 8, 10, and 11) to two areas. The eastern inner LCS was represented by the region inshore of 50 m and east of longitude 91.3°W (Figure 1). The western inner LCS was the defined as the region inshore of 50 m and west of 91.3°W. Longitude 91.3°W was selected as the budgeting boundary because it roughly bisects the LCS such that the lower Mississippi River should be the dominant freshwater forcing east of this longitude and the Atchafalaya River should be dominant west of the boundary. The mean westward transport across longitude 91.3°W was used to estimate the mean fraction of Mississippi River loads that was transported westward. The westward export of constituents from the total budget region (east+ west) was defined as the rate of westward transport across longitude 93.3°W, at depths < 50 m. Cross-shelf transports were calculated over the 50 m isobath boundary of the eastern and western budget regions. The 50 m isobath was selected due to this location being a point of near zero velocities owing to the mean circulation patterns of the shelf [*Nowlin et al*., 2005]. Budget results were also analyzed as summer (cruises in June 2003, June 2006, September 2006, and August 2007) and nonsummer (remaining cruises) means. Splitting the year into summer and nonsummer periods was based on previous observations of this mode of seasonal variability in circulation patterns [*Cochrane and Kelly*, 1986].

[32] The average freshwater transport across the western face (longitude 93.3°W) of the budget control volume (Figure 1) was $-19.2 \pm 3.4 \times 10^3$ m^3 s^{-1} (in the along-shelf direction, negative indicates transport to the west), which

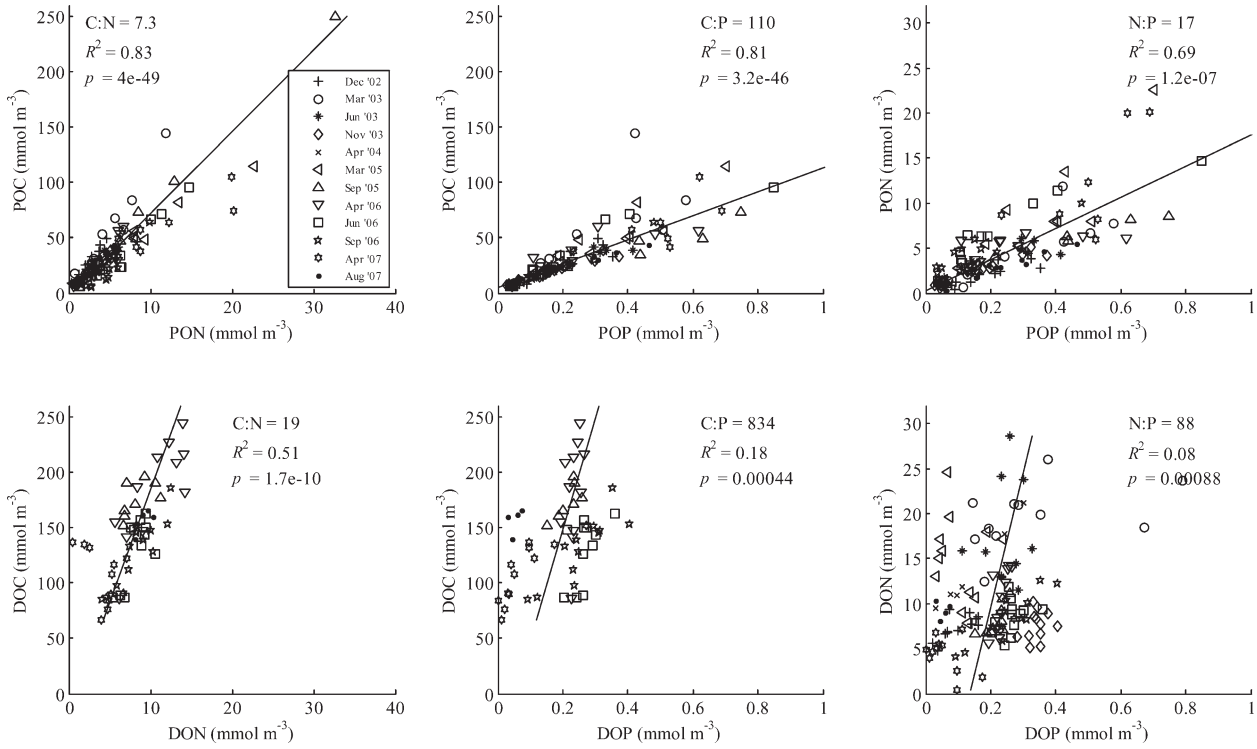

Figure 6. Stoichiometric ratios of particulate and dissolved organic C, N, and P. Regression lines are the results of model II regression analyses. Plotted values are mean values per budgeting region for the 12 cruises.

was approximately equal to the combined mean Mississippi and Atchafalaya River discharge of $19.2 \pm 0.2 \times 10^3$ m^3 s^{-1}. However, the transports were highly seasonal (Figure 10). During nonsummer months the mean freshwater transport across the western face was $-28.6 \pm 4.2 \times 10^3$ m^3 s^{-1}, while during summer the mean freshwater transport across this face was only $-8.7 \pm 2.1 \times 10^3$ m^3 s^{-1}. Interannual variation in the nonsummer westward transport was observed, which appeared to be related to the discharge such that highest river discharge resulted in greatest westward transport. However, the small number of observations prohibited a more thorough analysis of this pattern. Mean eastward transports of freshwater were calculated for June 2003 ($4.8 \pm 0.9 \times 10^3$ m^3 s^{-1}) and for August 2007 ($1.3 \pm 3.9 \times 10^3$ m^3 s^{-1}), while for the other two summer cruises (June and September 2006), the transports were directed westward but were smaller than during the nonsummer months (Figure 10).

[33] The mean cross-shelf transports at the 50 m isobath were generally directed northward. On the eastern shelf, in particular, the cross-shelf transports could be significant with calculated northward freshwater transport rates of $6.5 \pm 3.4 \times 10^3$ m^3 s^{-1}, equivalent to 33% of the mean MARB discharge. This large landward flux of freshwater across the 50 m isobath of the eastern shelf suggested transport of preexisting freshwater on the shelf.

[34] Overall, the average export rate of freshwater from the inner shelf was $21.6 \pm 3.6 \times 10^3$ m^3 s^{-1}. With an estimated freshwater volume of 110 km^3 for the budgeting region, the mean flushing time (volume/export rate) for freshwater would be 59 ± 10 days (Table 4). The seasonal changes in transports, however, resulted in very different flushing times of 120 ± 24 days during summer and 41 ± 7 days during nonsummer.

3.5. Calculated Nutrient Transports and Budgets

[35] Average transport of DIN across the western boundary was $-514 \pm 205 \times 10^3$ mmol s^{-1}, and DIN transport at this boundary was consistently smaller than MARB loads (on average, 25% of MARB) (Figure 10). Overall, the rivers were the dominant source of DIN to the LCS being approximately eightfold larger than the northward transports of DIN across the 50 m isobath. Mean DON transport across the western boundary was estimated to be $-1216 \pm 271 \times 10^3$ mmol s^{-1}, which was 2.8-fold larger than the combined DON load for Mississippi and Atchafalaya rivers of $436 \pm 16.5 \times 10^3$ mmol s^{-1}. The temporal pattern was similar to the freshwater transport, indicating the similar influence of the currents. In contrast to DIN, the rivers were not the dominant source of DON with the northward transport of DON across the 50 m isobath being 2.3-fold larger than the river DON loads.

[36] DIP and DOP inputs to the LCS also had large offshore components. The estimated transport of DIP northward across the 50 m isobath was 87% of the combined DIP river load of $37.3 \pm 1.4 \times 10^3$ mmol s^{-1} during the study period. While the average DOP transport northward at the 50 m isobath was approximately 2.4-fold larger than the combined Mississippi and Atchafalaya load of $8.4 \pm 0.4 \times 10^3$ mmol s^{-1}. Overall, though, for both TN and TP the riverine loads were the largest sources to the shelf (Figure 11) with the northward transport of TN and TP across the 50 m isobath being 50% and 44%, respectively, as large as the river loads.

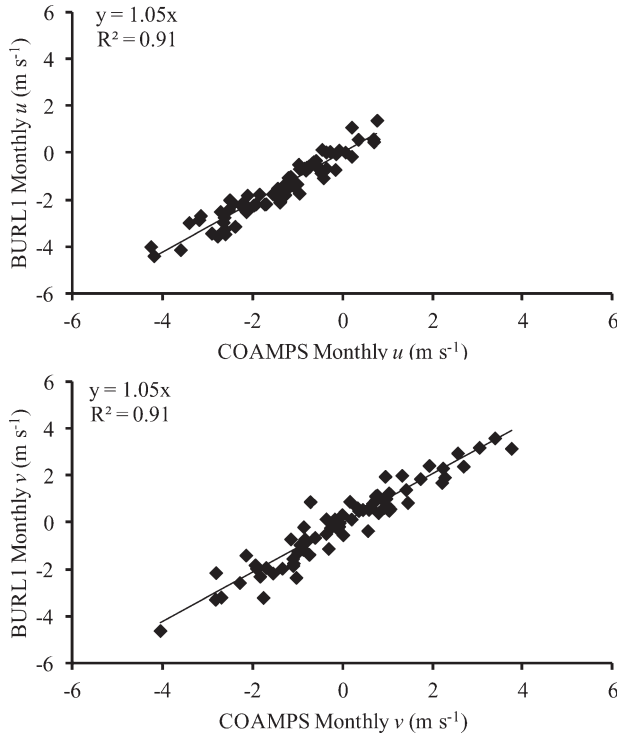

Figure 7. Comparison of monthly mean wind vectors (2002–2007) from buoy BURL1 (NOAA NDBC) to the COAMPS modeled wind at the location of BURL1. East-west (u, top) and north-south (v, bottom) observed and modeled wind vectors are shown. Regressions were fit with the intercept set equal to zero. Negative values of u were directed westward, negative values of v were directed southward.

[37] The mean steady-state budgets of TN and TP (Figure 11) indicated the inner shelf budget region was a net sink (equation (2)) for N and P, -3.15 ± 2.07 mmol N m^{-2} d^{-1} and -0.28 ± 0.08 mmol P m^{-2} d^{-1}, respectively. Large nonconservative sink rates calculated for the summer season (Table 4) occurred due to the summer time relaxation and reversal of currents on the inner shelf (Figure 5) resulting from the seasonal change in wind. This seasonal change in physical forcing resulted in the longest flushing times of N, P, and C during the summer season (Table 4). Summer flushing times ranged from 123 ± 26 days for TOC to 256 ± 4 days for DIN. In total, flushing times were shortest for organic N, P, and C and longest for DIN and DIP.

4. Discussion

4.1. Evaluation of NCOM-LCS

[38] Circulation patterns of the northern Gulf of Mexico are primarily wind driven [*Cochrane and Kelly*, 1986; *Oey*, 1995], and thus seasonal wind patterns are a dominant forcing of current directions and magnitudes. The mean circulation patterns produced by NCOM-LCS (Figure 3) were similar to previous studies that have observed mean westward currents and transport of freshwater on the inner shelf [*Cochrane and Kelly*, 1986; *Dinnel and Wiseman*, 1986; *Wiseman et al*., 1997; *Nowlin et al*., 2005]. Westward current velocities produced by NCOM-LCS for the inner shelf, mean $u = -2.2 \pm 0.03$ cm s^{-1}, were a little larger, but not statistically different, than previous observations of mean $u = -1.2 \pm 0.91$ cm s^{-1} for the same region, as calculated from current data presented by *Nowlin et al*. [2005].

[39] The model also accurately reproduced observed temporal and spatial variability in salinity and temperature (Figures 8 and 9), and the model had good skill at predicting salinity and temperature (ME = 0.64 and 0.94, respectively, where ME = 1 indicates perfect skill in reproducing observations). The model skill for salinity was similar to a previous modeling study of the LCS, which calculated a mean model skill for salinity of 0.46 [*Fennel et al*., 2011; *Hetland and DiMarco*, 2012].

[40] Modeled temperatures had more realistic vertical profiles and more closely matched observations after adding the enhancements to improve estimation of the surface heat flux. Initially, the use of an invariant *Jerlov* [1976] oligotrophic ocean water type 1A resulted in temperature profiles that differed from observations such that the model underpredicted the surface layer temperature and overpredicted temperature in the bottom layer. After modifying the model using the spatially explicit monthly time series of satellite-derived K_{PAR}, the surface layer absorbed more solar radiation and, thus, warmer temperatures were produced in the surface layer relative to the bottom, similar to observations (Figure 8). This solution addressed an identified deficiency in model skill to predict temperature for coastal

Table 4. Fill Times, Flushing Times, and Sink/Source Rates for Constituents (R_C) for the Inner Shelf Budget Region[a]

	Fall, Winter, Spring			Summer			All		
	Fill Time (d)	Flushing Time (d)	R_C (mmol m^{-2} d^{-1})	Fill Time (d)	Flushing Time (d)	R_C (mmol m^{-2} d^{-1})	Fill Time (d)	Flushing Time (d)	R_C (mmol m^{-2} d^{-1})
FW[b]	46	41	0.82	55	120	−2.75	49	59	−1.03
DIN	19	44	−2.81	19	256	−4.50	19	65	−3.51
DON	85	64	0.93	67	133	−1.81	79	82	−0.13
TN	51	51	0.07	37	125	−8.41	46	68	−3.15
DIP	41	61	−0.05	33	122	−0.13	38	73	−0.07
DOP	93	81	0.01	53	137	−0.05	75	92	−0.01
TP	35	73	−0.25	36	140	−0.34	35	86	−0.28
DOC	121	34	67.6	58	128	−30.1	86	59	17.0
TOC	107	33	83.4	52	123	−43.5	77	58	16.5

[a]Nonsummer and summer means were calculated from cruises that occurred during these seasons. Means from all the observations were also calculated. Propagated standard errors (not shown) were, on average, 30%, 21%, and 66% of fill times, flushing times, and R_C, respectively.
[b]Units are cm d^{-1} for sinks/sources of FW (i.e., R_{FW}), a negative R_C value indicates a sink rate and a positive value indicates a source rate.

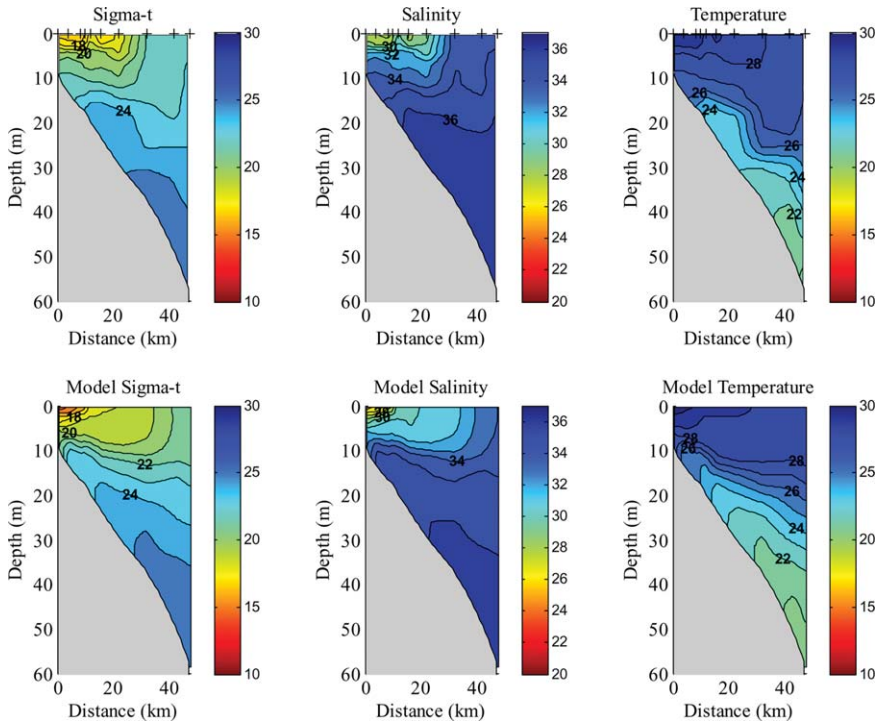

Figure 8. (top) June 2006 transect B cross-shelf profiles of sigma-t, salinity, and temperature. (bottom) Modeled hydrography for corresponding dates. From left to right are density (sigma-t), salinity, and temperature. Hatch marks on the upper axes of Figure 8 (top) indicate sampling locations used for interpolation. Contour lines = 1 unit.

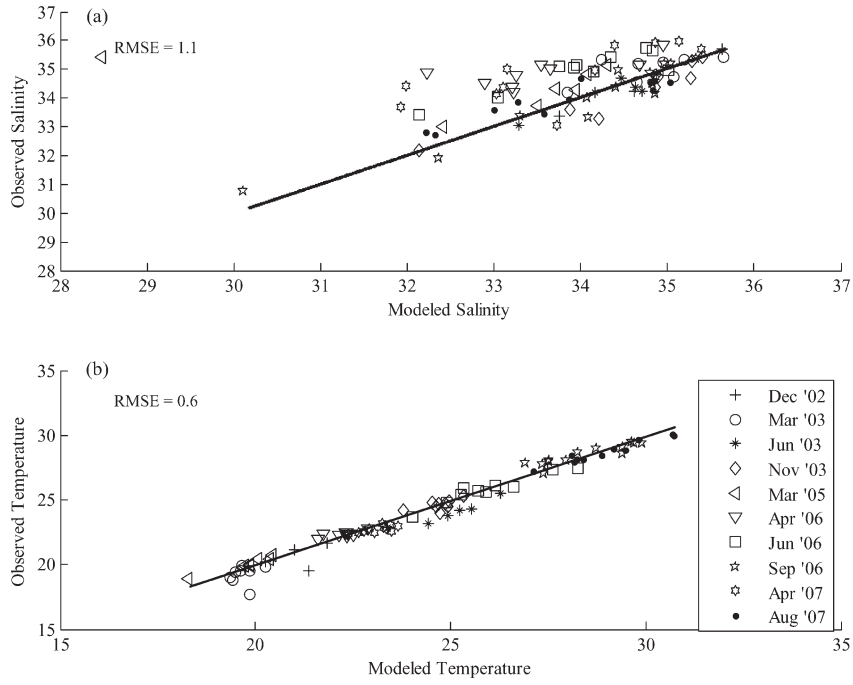

Figure 9. (a) Comparison of modeled average transect salinity to observed average transect salinity. (b) Comparison of modeled average transect temperature to observed average transect temperature. Black lines represent a 1:1 correspondence. Root-mean-square errors (RMSE) represent the mean error of the model in predicting observations.

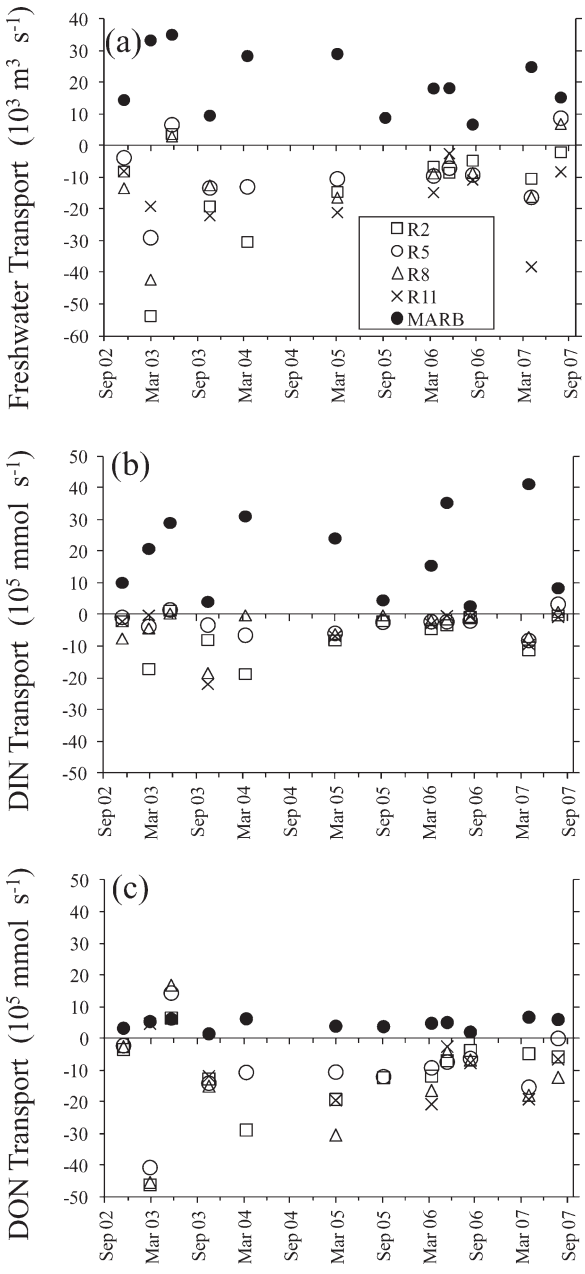

Figure 10. Combined Mississippi and Atchafalaya loads of (a) freshwater, (b) DIN, and (c) DON to the shelf and transports of these constituents (loads, 10^5 mmol s^{-1}) across the western faces of regions 2, 5, 8, and 11. River loads were treated as sources (positive values) and westward transports across the boundary faces were exports (negative values).

models using spatially uniform surface heat flux climatology [*Hetland and DiMarco*, 2012]. The net outcome of this model enhancement was that the modeled density profiles more closely matched the observed profiles than previous versions of the model, and, thus, better represented the observed pycnocline depth and strength (data not shown).

[41] Seasonal circulation patterns [*Cochrane and Kelly*, 1986] were reproduced by the model with nonsummer currents directed westward on the inner shelf and summer currents smaller and, in places, directed eastward. The seasonal changes in circulation resulted from a change in wind patterns from nonsummer, when winds were generally easterly, to summer months, when winds were primarily from the west. The circulation pattern on the eastern shelf is further complicated by the adjacent steep bathymetry of the shelf. The relatively deep waters near the Mississippi River discharge result in a surface-trapped plume that is detached from the bottom. Under these conditions, based on the Coriolis effect alone, it is expected that the plume will veer to the right until encountering a shoreline. With the addition of an ambient westward current west of the birdsfoot delta, a near geostrophic downcoast current should develop along the shelf, which could result in downcoast freshwater transports equal to river discharge [*Fong and Geyer*, 2002]. This appeared to be the case during nonsummer seasons when an estimated 65% of the Mississippi River freshwater discharge transited westward on the inner shelf.

4.2. Freshwater Transports

[42] On average, 47% of the lower Mississippi River freshwater discharge transited westward along the inner LCS, but this percentage varied seasonally with a mean of 65% during nonsummer months to variable, sometimes eastward transport during summer (Figure 10). The estimated 47% of Mississippi River freshwater transported westward was similar to previous estimates of 43% [*Etter et al*., 2004] and 53% [*Dinnel and Wiseman*, 1986]. The percentage transported westward is likely controlled by variation in winds, but the plume circulation is also affected by variation in river discharge and interaction with loop current eddies [*Walker et al*., 2005]. Further work is needed to understand how the variability in these forcing factors contributes to variability in along-shelf transports. This is important for understanding the impact of river constituent loads to the LCS, because the changes in the magnitude and direction of freshwater transport impact the amount of time that freshwater remains on the LCS.

[43] The average freshwater flushing time of the inner shelf was calculated to be 59 days (Table 4), setting a lower boundary for how long riverine nutrients may reside on the inner shelf. The average flushing time was similar in scale to the 1 month lag observed between nutrient inputs and maximum primary production on the eastern shelf [*Justić et al*., 1997] and the 2 month time lag that has been inferred from multivariate relationships between river discharge and nutrient concentrations, and midsummer shelf hypoxia areal extent [*Greene et al*., 2009].

[44] The summer current reversal on the inner shelf from westward to eastward resulted in very different freshwater flushing times for nonsummer and summer seasons (Table 4). Even with the interannual variability in transport rates and small sample sizes factored into the calculations of flushing time standard errors (Table 4, standard errors propagated to flushing and fill time estimates), summer versus nonsummer mean flushing times were significantly different. These results were consistent with observations of freshwater pooling on the eastern LCS during summer [*Cochrane and Kelly*, 1986; *Nowlin et al*., 2005]. As a consequence of the summer reversal, the flushing times for nutrients and organic matter increased during summer (Table 4), much more so than the change in freshwater

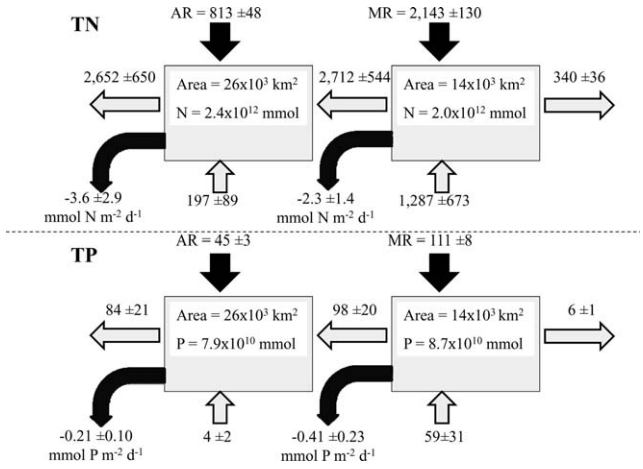

Figure 11. Mean steady-state TN and TP budgets for the eastern and western inner LCS. For budgeting analyses, the shelf was divided into eastern and western regions at the longitude 91.3°W. The budgets depict the TN and TP loads (10^3 mmol s^{-1}) from the rivers (black arrows) and the transport exchanges (10^3 mmol s^{-1}, gray arrows) over the 50 m isobath and along the shelf over the eastern boundary (88.8°W), western boundary (93.3°W), and middle boundary (91.3°W). Nonconservative sink rates (represented by the curved black arrows) were scaled to areal rates (mmol m^{-2} d^{-1}) based on the area of each region. Volume-normalized masses of N and P (mmol) in the eastern and western regions are also shown. Uncertainties are propagated standard errors.

flushing. Thus, it appeared that the physical trapping of riverine materials on the eastern LCS during summer, due to the reduction in the westward current velocity resulted in enhanced nonconservative removal of nutrients and organic matter (Table 4, discussed below).

4.3. Nutrient and Organic Carbon Distribution and Transport

[45] The nutrient and organic carbon samples from this study (Table 1) substantially add to the total sample size of available observations from the LCS (Table 5). Previously reported concentrations were primarily from the salinity gradient of the Mississippi River plume. Thus, the shelf-wide coverage provided here (Figure 1) expands the spatial coverage of observations considerably. Generally, though, nutrient and organic carbon observations were within reported ranges.

[46] DIN and DIP concentrations (Table 3) were driven by conservative mixing (Figure 4) and by uptake and regenerative processes (Figures 4 and 5) as modified by the seasonal changes in transport (Figure 10). Similar nonconservative uptake of inorganic nutrients and production of particulate and dissolved organic matter in midsalinity surface waters from this and other major river plume regions have been attributed to nutrient uptake into biomass and grazing processes [*Benner and Opsahl*, 2001; *Dagg et al*., 2004]. This is consistent with the TN and TP pools becoming more organic in composition (Table 3) at locations away from the plumes. Further evidence of the strong coupling of particulate nutrient dynamics to plankton biomass were the mean PC:PN, PC:PP, and PN:PP (Figure 6), which were similar to the Redfield ratio. These particulate stoichiometric ratios could be attributed to either phytoplankton or bacterial biomass, which have both been observed to have a mean C:N:P composition similar to Redfield [*Cotner et al*., 2010].

[47] In contrast, the stoichiometric ratios of dissolved organic matter constituents on the LCS were much larger than Redfield. Stoichiometric ratios of DOC:DON, DOC:DOP, and DON:DOP (Figure 6) were more similar to the rivers. The Mississippi River had DOC:DON, DOC:DOP, and DON:DOP of 14 ± 0.6, 700 ± 43, and 50 ± 10, respectively, and the Atchafalaya River had ratios of 16 ± 0.6, 810 ± 42, and 52 ± 9.3, respectively. Besides contributions from the rivers and remineralization of PC, the dissolved organic pools are composed of organic matter from adjacent marshes [*Bianchi et al*., 2011] and potentially from contributions of offshore DOC (Table 3). Regardless of source, due to DOC being the dominant organic form, the significant removal of LCS dissolved organic matter by photooxidation (the dominant loss term) and microbial remineralization [*Fichot and Benner*, 2012] represents a large turnover of dissolved organic matter.

Table 5. By Salinity, Ranges of DIN, DON, PN, DIP, DOP, PP, DOC, and POC Observed[a]

	Salinity Bin	DIN[b,c]	DON[d]	PN	DIP[b,c]	DOP[e,f]	PP	DOC[g,h]	PC[i]
Present Study	<18	2.7–164	0–46	1.8–38	0.04–2.8	0–3.2	0.1–1.8	150–335	30–156
	18–32	0–60	0–99	0–89	0–1.7	0–5.9	0–3.2	62–485	10–417
	>32	0–36	0–55	0–71	0–3.2	0–1.2	0–2.2	34–347	2–222
Previous Studies	<18	0–200	24–39	NA	1–6	0.17–2.4	NA	100–450	0–600
	18–32	0–107	3–50	NA	0.05–4	0.07–1.8	NA	80–390	0–90
	>32	0–20	2–36	NA	0.01–1	0.05–0.03	NA	60–159	0–25

[a]Concentration units are mmol m^{-3}. Ranges reported from previous studies were obtained from references as indicated in subsequent footnotes.
[b]*Lohrenz et al*. [1999]
[c]*Chen et al*. [2000]
[d]*Lopez-Veneroni and Cifuentes* [1994]
[e]*Rinker and Powell* [2006]
[f]*Cai and Guo* [2009]
[g]*Benner and Opsahl* [2001]
[h]*Wang et al*. [2004]
[i]*Trefry et al*. [1994]. Note: PC concentrations given by *Trefry et al*. [1994] were not presented by salinity, and thus salinity were inferred from sampling locations in relation to the mean salinity observed in the present study. NA = no available data from previous efforts.

[48] Based on a cross-system meta-analysis of microbial DOM lability by *del Giorgio and Davis* [2003], DOM from riverine, estuarine, and marine systems has mean turnover rates of 12%, 15%, and 26% over a 20 day period, respectively. To examine the potential range of microbial DOC turnover rates on the LCS, we applied the three different turnover rates to the mean DOC concentration (147 mmol m^{-3}) for the inner shelf (<50 m depth). This yielded potential microbial DOC remineralization rates ranging from 0.9 to 1.9 mmol C m^{-3} d^{-1}. Based on mean observed surface and bottom water respiration rates of 10 and 5 mmol O_2 m^{-3} d^{-1}, respectively, for the LCS [*Murrell et al*., 2013], the estimated DOC remineralization rates (assuming $C:O_2 = 1$) could represent 9–19% of mean surface water respiration and 18–38% of mean bottom water respiration. This simple scaling analysis suggests that DOC contributions to respiration may be significant, but, on average, are likely to be a lesser contribution than PC. Because PC on the inner LCS (mean = 67 mmol C m^{-3}) has a smaller concentration than DOC, the turnover rates for PC would have to be much larger than for DOC. Future studies are needed to better quantify the multiple end-member sources of DOC and POC and attribute their contributions to total inner shelf respiration.

[49] Surprisingly, the calculated DOC, DON, and DOP inputs northward across the 50 m isobath were 1.5, 2.3, and 2.4-fold larger than the river load inputs, with the large majority (>95%) of this northward transport occurring east of longitude 90.3°W. The origin of the offshore-dissolved organic nutrients is likely "aged" carbon based on the mean stoichiometry (Figure 6), and the source could be the open Gulf of Mexico or preexisting freshwater on the shelf. The mean onshore-directed transport of freshwater on the eastern shelf was large, 33% of the MARB discharge, and supports the idea of preexisting freshwater. This preexisting freshwater could be river water that has transited the inner shelf westward to the Texas shelf and then returned eastward via transport on the outer shelf. This transport pattern has been previously hypothesized to explain the formation of secondary, near-bottom density stratification [*Wiseman et al*., 1997].

[50] Despite the large organic nutrient loads from offshore, the Mississippi and Atchafalaya rivers were the dominant sources of TN and TP to the inner LCS owing to the large inorganic and particulate nutrient loads delivered by the rivers. The dominant export pathway from the shelf was transport at the western boundary, consistent with the mean current direction of the Louisiana coastal current [*Wiseman et al*., 1997], the direct discharge of the Atchafalaya River, and the expected along-shelf transport behavior of the Mississippi River plume [*Fong and Geyer*, 2002].

4.4. Nutrient Budgets

[51] Previous N budgeting studies for the LCS have also concluded that the MARB is the dominant source [*Walsh et al*., 1989; *Nixon et al*., 1996]. This is a unique situation for the continental shelf. *Nixon et al*. [1996] produced N budgets for the shelf systems of the North Atlantic and found that all the systems except the LCS were dominated by offshore nutrient sources. Clearly, as the spatial scale of analysis increases in the coastal ocean, the open ocean influence becomes greater. However, at the scale of the inner LCS, where riverine nutrients are implicated in the development of hypoxia [*Rabalais et al*., 2002; *Bianchi et al*., 2010], the dominant source of N and P is the MARB (Figure 11).

[52] The mean steady-state TN budget (Figure 11) suggested the inner shelf was a net N sink (calculated from equation (2)) in the amount of -3.15 ± 2.07 mmol N m^{-2} d^{-1}. This N sink represented 33% of the total nitrogen delivered to the inner shelf from both riverine and offshore sources. The calculated N sink ± uncertainty was higher than, but in the range of, denitrification rates observed at sites on the inner LCS, which had site average rates ranging from −2.8 to −0.9 mmol N m^{-2} d^{-1} [*Lehrter et al*., 2012]. Similarly, the inner shelf was also a net sink of TP in the amount of -0.28 ± 0.08 mmol P m^{-2} d^{-1}. The rapid removal of P at low salinity (Figure 4) must occur due to burial in the lower river reaches or in shallow areas adjacent to the plumes [*Sutula et al*., 2004]. The burial sink of P, which is more particle reactive than N and thus more prone to be buried, could be supported by the large sedimentation rates (>10 cm yr^{-1}) occurring in and adjacent to the delta lobes of the lower Mississippi and Atchafalaya rivers [*Chen et al*., 2005], whereas more distant from the river sedimentation rates for the inner shelf were 0.1–0.4 cm yr^{-1}.

[53] In sum, the observed spatial patterns of salinity and nutrients suggest that most of the initial riverine nutrient uptake and organic matter production is occurring in waters immediately adjacent to the points of freshwater discharge. Subsequently, the organic matter is exported away from the river plume regions as dissolved organic material, where it contributes to recycled production and the net heterotrophy observed for most of the shelf [*Murrell et al*., 2013]. Seasonal changes in circulation result in enhanced inner shelf retention and nonconservative uptake of nutrients and organic matter during the summer. However, during nonsummer, the mean circulation carried the bulk of the river nutrients westward and ultimately exported them to the Texas shelf via the coastal boundary current.

[54] Other potential N sources should also be more thoroughly accounted in future studies conducted at finer spatial and temporal scales. For example, though atmospheric deposition is considered a small source in comparison to the mean river discharge, it may be seasonally important during low discharge periods like fall and winter. During these seasons, precipitation directly to the surface water of the LCS becomes a much bigger freshwater source proportional to river discharge [*Dinnel and Wiseman*, 1986].

5. Conclusions

[55] We investigated the transports, transformations, and sinks of nutrients from the Mississippi River watershed on the LCS using observational data and results from a high-resolution, coastal circulation model, and mean budgets of TN and TP were calculated for the period 2002–2007. This is the first attempt to analyze in a budgeting framework the physical transports and sources and sinks affecting the distribution and speciation of nutrients on the LCS.

[56] The seasonal patterns of nutrient transport were consistent with the mean wind fields. Westward transports occurred during nonsummer months when prevailing winds were from the east, while nutrients and organic matter were

often transported eastward during summer associated with prevailing winds from the southwest. This seasonal reversal of currents has a large effect on the flushing times of nutrients from the LCS and contributes to the accumulation of nutrients and organic matter on the inner shelf coincident with the drawdown of bottom water oxygen.

[57] The result that physical forcing played such a significant role in the magnitude of biogeochemical transformations and sinks for N, P, and C was novel for the LCS. This suggested that interannual variability in winds and, hence, downcoast currents could be an important mediator of shelf N, P, and C. Winds are predicted to change due to climate change [*IPCC*, 2007]; which, if prevailing winds strengthen, may help to alleviate the nutrient issue on the LCS by more rapidly transporting nutrients downcoast during spring or may exacerbate the nutrient and hypoxia issue by increasing the retention time on the shelf during the summer months.

[58] The results from this study, however, should be interpreted cautiously owing to large propagated uncertainties calculated for the budgeting terms. The limited sample size ($n = 12$ cruises) for the analyses was the primary contributing factor to this uncertainty and suggests that more frequent sampling is needed to reduce contributions of temporal and spatial uncertainties. Future budgeting efforts are also needed, and should aim to increase the temporal and spatial resolution through improved sampling or by implementing validated, coupled hydrodynamic-ecosystem models to examine nutrient and metabolic responses to river, wind, and offshore eddy forcing. Finer spatial scale analyses are also needed to examine the dynamics of potential nutrient and organic matter source and sink end-members (the Mississippi and Atchafalaya river distributaries, the coastal marshes and bays, offshore waters, atmospheric deposition, N fixation, and denitrification) and their contributions to the balance of primary production and respiration.

[59] **Acknowledgments.** We thank Jessica Aukamp, David Beddick, Brandon Jarvis, Roman Stanley, and Diane Yates for sample processing, laboratory analyses, and database assistance. We thank the crews of the OSV *Anderson*, RV *Longhorn*, and OSV *Bold* for their assistance on cruises. We thank Harvey Seim and two anonymous reviewers for constructive comments on an earlier draft. This work was supported by the U.S. EPA Office of Research and Development and the U.S. IOOS Coastal Ocean Modeling Testbed. The study was reviewed and approved for publication by the U.S. EPA National Health and Environmental Effects Research Laboratory; however, the contents are solely the views of the authors. Use of trade names of commercial products does not constitute endorsement by the U.S. EPA.

References

APHA (1989), *Standard Methods for the Examination of Water and Wastewater*, 17th ed., Am. Public Health Assoc., Washington, D. C.

Benner, R., and S. Opsahl (2001), Molecular indicators of the sources and transformations of organic matter in the Mississippi river plume, *Org. Geochem.*, *32*, 597–611.

Bianchi, T. S., S. F. DiMarco, J. H. Cowan, R. D. Hetland, P. Chapman, J. W. Day, and M. A. Allison (2010), The science of hypoxia in the northern Gulf of Mexico: A review, *Sci. Total Environ.*, *408*, 1471–1484, doi:10.1016/j.scitotenv.2009.11.047.

Bianchi, T. S., L. A. Wysocki, K. M. Schneider, T. R. Filley, D. R. Corbett, and A. Kolker (2011), Sources of terrestrial organic carbon in the Mississippi Plume region, *Aquat. Geochem.*, *17*, 431–456, doi:10.1007/s10498-010-9110-3.

Cai, W-J., Z. A. Wang, and Y. Wang (2003), The role of marsh-dominated heterotrophic continental margins in transport of CO_2 between the atmosphere, the land-sea interface, and the ocean, *Geophys. Res. Lett.*, *30*(16), 1849, doi:10.1029/2003GL017633.

Cai, Y., and L. Guo (2009), Abundance and variation of colloidal organic phosphorus in riverine, estuarine, and coastal waters in the northern Gulf of Mexico, *Limnol. Oceanogr.*, *54*, 1393–1402.

Chen, X., S. E. Lohrenz, and D. A. Wiesenburg (2000), Distribution and controlling mechanisms of primary production on the Louisiana-Texas continental shelf, *J. Mar. Syst.*, *25*, 179–207.

Chen, N., T. S. Bianchi, and B. A. McKee (2005), Early diagenesis of chloropigment biomarkers in the lower Mississippi River and Louisiana shelf: Implications for carbon cycling in a river-dominated margin, *Mar. Chem.*, *93*, 159–177.

Cochrane, J. D., and F. J. Kelly (1986), Low-frequency circulation on the Texas-Louisiana continental shelf, *J. Geophys. Res.*, *91*, 10,645–10,659.

Cotner, J. B., E. K. Hall, J. T. Scott, and M. Heldal (2010), Freshwater bacteria are stoichiometrically flexible with a nutrient composition similar to seston, *Front. Microbiol.*, *1*, 132, doi:10.3389/fmicb.2010.00132.

Dagg, M. J., and G. A. Breed (2003), Biological effects of Mississippi River nitrogen on the northern Gulf of Mexico—A review and synthesis, *J. Mar. Syst.*, *43*, 133–152, doi:10.1016/j.marsys.2003.09.002.

Dagg, M., R. Benner, S. Lohrenz, and D. Lawrence (2004), Transformation of dissolved and particulate materials on continental shelves influenced by large rivers: Plume processes, *Cont. Shelf Res.*, *24*, 833–858, doi:10.1016/j.csr.2004.02.003.

del Giorgio, D., and J. Davis (2003), Patterns in dissolved organic matter lability and consumption across aquatic ecosystems, in *Aquatic Ecosystems: Interactivity of Dissolved Organic Matter*, edited by S. E. G Findlay and R. L. Sinsabaugh, pp. 399–324, Academic, San Diego, Calif.

Diaz, R. J, and R. Rosenberg (2008), Spreading dead zones and consequences for marine ecosystems, *Science*, *321*, 926–929, doi:10.1126/science.1156401.

Dinnel, S. P., and W. J. Wiseman (1986), Fresh water on the Louisiana and Texas shelf, *Cont. Shelf Res.*, *6*, 765–784.

Dunn, D. D. (1996), Trends in nutrient inflows to the Gulf of Mexico from streams draining the conterminous United States 1972–1993, *Water Resour. Invest. Rep. 96–4113*, U.S. Geol. Surv., Austin, Texas.

Etter, P. C., M. K. Howard, and J. D. Cochrane (2004), Heat and freshwater budgets of the Texas-Louisiana shelf, *J. Geophys. Res.*, *109*, C02024, doi:10.1029/2003JC001820.

Fennel, K., R. Hetland, Y. Feng, and S. DiMarco (2011), A coupled physical-biological model of the Northern Gulf of Mexico shelf: Model description, validation and analysis of phytoplankton variability, *Biogeosciences*, *8*, 1881–1899, doi:10.5194/bg-8–1881-2011.

Fennel, K., J. Hu, A. Laurent, M. Marta-Almeida, and R. Hetland (2013), Sensitivity of hypoxia predictions for the northern Gulf of Mexico to sediment oxygen consumption and model nesting, *J. Geophys. Res.*, *118*, 990–1002, doi:10.1002/jgrc.20077.

Fichot, C. G., and R. Benner (2012), The spectral slope coefficient of chromophoric dissolved organic matter ($S_{275–295}$) as a tracer of terrigenous dissolved organic carbon in river-influenced margins, *Limnol. Oceanogr.*, *37*, 1453–1466, doi:10.4319/lo.2012.57.5.1453.

Fong, D. A., and W. R. Geyer (2002), The alongshore transport of water in a surface-trapped river plume, *J. Phys. Oceanogr.*, *32*, 957–972.

Goolsby, D. A., W. A. Battaglin, G. B. Lawrence, R. S. Artz, B. T. Aulenbach, R. P. Hopper, D. R. Keeney, and G. J. Stensland (1999), Flux and sources of nutrients in the Mississippi-Atchafalaya River basin, Topic 3 report for the integrated assessment on hypoxia in the Gulf of Mexico, *Decision Anal. Ser. 17*, NOAA Coastal Ocean Program, Silver Spring, Md.

Greene, R. M., J. C. Lehrter, and J. D. Hagy (2009), Multiple regression models for hindcasting and forecasting midsummer hypoxia in the Gulf of Mexico, *Ecol. Appl.*, *19*, 1161–1175.

Hetland, R. D., and S. F. DiMarco (2012), Skill assessment of a hydrodynamic model of circulation over the Texas-Louisiana continental shelf, *Ocean Modell.*, *43–44*, 64–76, doi:10.1016/j.ocemod.2011.11.009.

Holmes, R. M., A. Aminot, R. Kerouel, B. A. Hooker, and B. J. Peterson (1999), A simple and precise method for measuring ammonium in marine and freshwater ecosystems, *Can. J. Fish. Aquat. Sci.*, *56*, 1801–1808.

IPCC (2007), *Climate Change 2007: Synthesis Report, Contribution of Working Groups I, II, and III to the Fourth Assessment Report of the Intergovernmental Panel on Climate Change*, edited by R. K. Pachauri and A. Reisinger, pp. 26–73, IPCC, Geneva, Switzerland.

Jerlov, N. G. (1976), *Marine Optics*, Elsevier Sci., Amsterdam.

Jolliff, J., T. A. Smith, C. Barron, S. deRada, S. C. Anderson, R. W. Gould, and R. A. Arnone (2012), The impact of coastal phytoplankton blooms on ocean-atmosphere thermal energy exchange: Evidence from a two-way coupled numerical modeling system, *Geophys. Res. Lett.*, *39*, L24607, doi:10.1029/2012GL053634.

Justić, D., N. N. Rabalais, and R. E. Turner (1997), Impacts of climate change on net productivity of coastal waters: Implications for carbon budgets and hypoxia, *Clim. Res.*, *8*, 225–237.

Justić, D., V. J. Bierman, D. Scavia, and R. D. Hetland (2007), Forecasting Gulf's hypoxia: The next 50 years, *Estuaries Coasts*, *30*, 791–801.

Ko, D. S., R. H. Preller, and P. J. Martin (2003), An experimental real-time intra-Americas sea ocean nowcast/forecast system for coastal prediction, paper presented at AMS 5th Conference on Coastal Atmospheric and Oceanic Prediction and Processes, AMS, Seattle, Wash.

Ko, D. S., P. J. Martin, C. D. Rowley, and R. H. Preller (2008), A real-time coastal ocean prediction experiment for Mississippi RiverEA04, *J. Mar. Syst.*, *4*, 17–28, doi:10.1016/j.jmarsys.2007.02.022.

Lee, Z. P., K. P. Du, and R. Arnone (2005), A model for the diffuse attenuation coefficient of downwelling irradiance, *J. Geophys. Res.*, *110*, C02016, doi:10.1029/2004JC002275.

Lehmann, M. K., K. Fennel, and R. He (2009), Statistical validation of a 3-D bio-physical model of the western North Atlantic, *Biogeosciences*, *6*, 1961–1974.

Lehrter, J. C., and J. Cebrian (2010), Uncertainty propagation in an ecosystem nutrient budget, *Ecol. Appl.*, *20*, 508–524.

Lehrter, J. C., D. L. Beddick, R. Devereux, D. F. Yates, and M. C. Murrell (2012), Sediment-water fluxes of dissolved inorganic carbon, O_2, nutrients, and N_2, from the hypoxic region of the Louisiana continental shelf, *Biogeochemistry*, *109*, 233–252, doi:10.1007/s10533-011-9623-x.

Lohrenz, S. E., G. L. Fahnenstiel, D. G. Redalje, G. A. Lang, M. J. Dagg, T. E. Whitledge, and Q. Dortch (1999), Nutrients, irradiance, and mixing as factors regulating primary production in coastal waters impacted by the Mississippi River plume, *Cont. Shelf Res.*, *19*, 1113–1141.

Lohrenz, S. E., D. G. Redalje, W.-J. Cai, J. Acker, and M. Dagg (2008), A retrospective analysis of nutrients and phytoplankton productivity in the Mississippi River plume, *Cont. Shelf Res.*, *28*, 1466–1475.

Lopez-Veneroni, D., and L. A. Cifuentes (1994), Transport of dissolved organic nitrogen in Mississippi river plume and Texas-Louisiana continental shelf near-surface waters, *Estuaries*, *17*, 796–808.

Martin, P. J. (2000), Description of the navy coastal ocean model version 1.0, NRL/FR/7322–00–9962, Naval Res. Lab., Stennis Space Center, Miss.

Menzel, D. (1965), The measurement of total phosphorus in seawater based on the liberation of organically bound fractions by persulfate oxidation, *Limnol. Oceanogr.*, *10*, 280–282.

Murrell, M. C., and J. C. Lehrter (2011), Sediment and lower water column oxygen consumption in the seasonally hypoxic region of the Louisiana continental shelf, *Estuaries Coasts*, *34*, 912–924, doi:10.1007/s12237-010-9351-9.

Murrell, M. C., R. S. Stanley, J. C. Lehrter, and J. D. Hagy (2013), Plankton community respiration, net ecosystem metabolism, and oxygen dynamics on the Louisiana continental shelf: Implications for hypoxia, *Cont. Shelf Res.*, *52*, 27–38, doi:10.1016/j.csr.2012.10.010.

Nixon, S. W., et al. (1996), The fate of nitrogen and phosphorus at the land-sea margin of the North Atlantic Ocean, *Biogeochemistry*, *35*, 141–180.

Nowlin, W. D., Jr., A. E. Jochens, S. F. DiMarco, R. O. Reid, and M. K. Howard (2005), Low-frequency circluation over the Texas-Louisiana continental shelf, in *Circulation in the Gulf of Mexico: Observations and Models, Geophys. Monogr. Ser*., vol. *161*, edited by W. Sturgers and A. Lugo-Fernandes, pp. 203–218, AGU, Washington, D. C.

Oey, L.-Y. (1995), Eddy- and wind-forced shelf circulation, *J. Geophys. Res.*, *100*, 8621–8637.

Pond, S., and G. L. Pickard (1983), *Introductory Dynamical Oceanography*, 2nd ed., Pergamon, Oxford.

Rabalais, N. N., R. E Turner, and W. J. Wiseman (2002), Gulf of Mexico hypoxia, A.K.A. "The Dead Zone," *Annu. Rev. Ecol. System.*, *33*, 235–263, doi:10.1146/annurev.ecolsys.33.010802.150513.

Riley, G. A. (1937), The significance of the Mississippi River drainage for biological conditions in the northern Gulf of Mexico, *J. Mar. Res.*, *1*, 60–74.

Rinker, K. R., and R. T. Powell (2006), Dissolved organic phosphorus in the Mississippi River plume during spring and fall 2002, *Mar. Chem.*, *102*, 170–179, doi:10.1016/j.marchem.2005.09.013.

Sahl, L. E., W. J. Merrell, and D. C. Biggs (1993), The influence of advection on the spatial variability of nutrient concentrations on the Texas-Louisiana continental shelf, *Cont. Shelf Res.*, *13*, 233–251.

Schaeffer B. A., G. A. Sinclair, J. C. Lehrter, M. C. Murrell, J. C. Kurtz, R. W. Gould Jr. (2012), An analysis of diffuse light attenuation in the northern Gulf of Mexico hypoxic zone using the SeaWiFS satellite data record, *Remote Sens. Environ.*, *115*, 3748–3757.

Schiller, R. V., V. H. Kourafalou, P. Hogan, and N. D. Walker (2011), The dynamics of the Mississippi River plume: Impact of topography, wind, and offshore forcing on the fate of plume waters, *J. Geophys. Res.*, *116*, C06029, doi:10.1029/2010JC006883.

Sharp, J. (1973), Total organic carbon in seawater—Comparison of measurements using persulfate oxidation and high temperature combustion, *Mar. Chem.*, *1*, 211–229.

Sharp, J. (1974), Improved analysis for "particulate" organic carbon and nitrogen from seawater, *Limnol. Oceanogr.*, *19*, 984–989.

Sutula, M., T. S. Bianchi, and B. A. McKee (2004), Effect of seasonal sediment storage in the lower Mississippi River on the flux of reactive particulate phosphorus to the Gulf of Mexico, *Limnol. Oceanogr.*, *49*, 2223–2235.

Sylvan, J. B., Q. Dortch, D. M. Nelson, A. F. Maier Brown, W. Morrison, and J. W. Ammerman (2006), Phosphorus limits phytoplankton growth on the Louisiana shelf during the period of hypoxia formation, *Environ. Sci. Technol.*, *40*, 7548–7553, doi:10.1021/es061417t.

Trefry, J. H., S. Metz, T. A. Nielsen, R. P. Trocine, and B. J. Eadie (1994), Transport of particulate organic carbon by the Mississippi River and its fate in the Gulf of Mexico, *Estuaries*, *17*, 839–849.

Turner, R. E., N. N. Rabalais, and D. Justić (2006), Predicting summer hypoxia in the northern Gulf of Mexico: Riverine N, P, and Si loading, *Mar. Pollut. Bull.*, *52*, 139–148.

Walker, N. D., W. J. Wiseman, L. J. Rouse, and A. Babin (2005), Effects of river discharge, wind stress, and slope eddies on circulation and the satellite-observed structure of the Mississippi River plume, *J. Coastal Res. 21*, 1228–1244.

Walsh, J. J., D. A. Dieterle, M. B. Meyers, and F. Müller-Karger (1989), Nitrogen exchange at the continental margin: A numerical model study, *Prog. Oceanogr.*, *23*, 245–301.

Wang, X.-C., R. F. Chen, and G. B. Gardner (2004), Sources and transport of dissolved and particulate organic carbon in the Mississippi River estuary and adjacent coastal waters of the northern Gulf of Mexico, *Mar. Chem.*, *89*, 241–256, doi:10.1016/j.marchem.2004.02.014.

Wiseman, W. J., N. N. Rabalais, R. E. Turner, S. P. Dinnel, and A. MacNaughton (1997), Seasonal and interannual variability within the Louisiana coastal current: Stratification and hypoxia, *J. Mar. Syst.*, *12*, 237–248.

Zhang, X., R. D. Hetland, M. Marta-Almeida, and S. F. DiMarco (2012), A numerical investigation of the Mississippi and Atchafalaya freshwater transport, filling and flushing times on the Texas-Louisiana shelf, *J. Geophys. Res.*, *117*, C11009, doi:10.1029/2012JC008108.